
Holocene stratigraphic architecture of a Mediterranean delta and implication for sediment budget evolution: Example of the Rhône delta

Martinez Théo ^{1, 2, *}, Deschamps Rémy ¹, Amorosi Alessandro ³, Jouet Gwenael ⁴, Vella Claude ⁵, Ducret Gabriel ¹, Berger Jean-François ²

¹ IFP Energies Nouvelles, 1-4 Avenue Bois Préau, 92500, Rueil-Malmaison, France

² CNRS, UMR 5600 EVS/IRG, Université Lyon 2, 18 rue Chevreul, 69362, Lyon, France

³ Dipartimento di Scienze Biologiche, Geologiche ed Ambientali, Università di Bologna, 33 Via Zamboni, Bologna, Italy

⁴ IFREMER, 1625 route de Sainte-Anne, 29280, Plouzané, France

⁵ Aix Marseille Univ, CNRS, IRD, INRA, Coll France, CEREGE, Aix-en-Provence, France

* Corresponding author : Théo Martinez, email address : theo.martinez@ifpen.fr

Abstract :

Deltaic systems evolve as a result of interactions between the hydroclimatic processes that occur in the catchment area and the coastal marine processes that reshape the coastline. The Holocene evolution of these environments is controlled by climate and anthropization, which are rarely considered in models of the evolution of deltaic systems. The Rhône delta has recorded the impact of climatic variations as well as the development and evolution of human societies over the Holocene period. This system underwent a post-glacial evolution controlled by global climatic warming punctuated by short periods of cooling, fluvial metamorphoses and a rapid marine transgression generated by the melting of the ice caps, followed by the initiation of delta progradation from around 7000 Cal yr BP. Sedimentological and chronostratigraphic studies of 17 cores, supplementing an existing dataset on the deltaic plain and the prodelta, have enabled us to construct well-constrained stratigraphic correlations, making it possible to specify the spatio-temporal evolution of the Rhône delta. The variation in sedimentary fluxes was assessed for the different sequences identified, using 95 new core datings to constrain the sequential evolution of the different lobes. From the stratigraphic correlations on the delta and the estimated volumes of sediments exported out of the deltaic system, the total sediment volume between 11,700 Cal yr BP and today is estimated at 126 billion cubic meters. The variation of sediment fluxes has been adjusted according to the different phases of lobes progradation linked with the climate oscillations and the anthropic activities evolution during the Holocene. Taken together, these data highlight contrasting periods corresponding to the Roman period, the Little Ice Age and finally the 'Anthropocene', that can be compared to the main Mediterranean deltaic systems during the Holocene.

Keywords : Rhône France, Holocene, Deltaic system, Chronostratigraphy, Sediment flow

1. Introduction

Environments at the interface between land and sea are vulnerable to the effects of climate change. Coasts include different environments such as cliffs, bays, deltas, and peninsulas, and coastal erosion presents a major challenge to the preservation of these environments. Among them, bays, estuaries, and deltas present a very low topography, and are therefore extremely sensitive to sea level rise caused by global warming. Projections by the IPCC (Intergovernmental Panel on Climate Change) for the year 2100 indicate a rise of 0.25 m compared with today for the most optimistic simulation, and up to 0.7 m for the most pessimistic (IPCC, 2022).

Deltas cover 5% of the total continental surface area and are host to 500 million people and rich ecosystems (Renaud and Kuenzer, 2012). The gradual disappearance of deltas could therefore lead to the displacement of large populations worldwide. The problems associated with the displacement of this population are complex and present a major short-term challenge.

Among low-topography coastal environments, deltas are particularly sensitive to future changes. On the ocean side, eustatic movements control the phases of delta progradation or retrogradation, and wave orientation and wavelength also impact delta morphology by reworking sediments along the coast. All the parameters controlling the evolution of deltas are likely to be modified by future climate change. A sea-level rise of 0.7 m would result in an average coastline retreat of 30 m for deltas (mean slope = 2.5° (McPherson et al., 1987)). On the continental side, the development of deltas is dependent on sediment transported by the river systems that drain their watersheds, with the quantity and type of sediment being the major parameters controlling their morphological evolution. Since the sedentarization of human communities around 7000 Cal yr BP in the Mediterranean, land use has been modified for the benefit of agriculture (Berger et al., 2019; Stanley and Warne, 1993). The development of agriculture has tended to increase the amount of sediment supplied in deltaic systems due to denudation of lands and the reworking of soils, processes that have favored erosion (Morgan, 2009). The accentuation of this phenomenon at basin scales in Western Europe is associated with proto-urbanization and the rise of metallurgy (Notebaert and Berger 2014). Although Roman and medieval societies experimented with hydraulic engineering on local scales, since the middle of the 20th century, river sediment transport has been disrupted from upstream to downstream by the development of hydraulic dams that rapidly modify fluvial styles (Petts and Gurnell, 2005). The amount of sediment supplied in deltas has decreased by around 50% to 80% (Nicholls et al., 2020) in highly anthropized watersheds, mainly due to the installation of dams. The coupling between sea-level rise and decrease in sediment supply is likely to induce retrogradation of deltaic systems, leading to numerous changes in terms of agricultural potential, drinking water, and other water-based resources.

The subsidence of deltas is another aggravating parameter. These areas of sediment accumulation have a natural tendency to subside due to the loading and compaction of deposited sediments (Coleman et al., 1998). In addition, large volume extractions of water or hydrocarbon resources in certain deltas also accentuate subsidence.

To limit the risks of coastal erosion or flooding of delta plains worldwide, land management is required. To counterbalance the reduction in solid loads carried by rivers due to upstream dams, the channel can be straightened to facilitate the transport of the solid fraction (Jauzein, 1971). To limit coastal erosion, dikes can be installed to induce a gradual change in the direction of the river mouth, encouraging sedimentation rather than export of sediment by swell at the river mouth.

Several deltaic systems can be found along the Mediterranean rim, particularly in the western part (Anthony et al., 2014). These deltas shared a comparable dynamic during the Holocene. The last glacial maximum (LGM; 20000 yr BP) caused a significant drop in sea level, and since then, a marine transgression has been recorded across the entire Mediterranean Sea (Berné et al., 2007; Amorosi et al., 2017). Sea level rise is recorded by the retrograding deposits in the deltas. When the sea level stabilized, the deltas were able to begin to prograde (Anthony et al., 2014). This inversion occurred at different periods: 8000 to 7500 Cal yr BP for the Nile delta (Pennington et al., 2017), 7600 to 6000 Cal yr BP for the Rhône delta (Vella et al., 2003; Arnaud-Fassetta and Suc, 2015), 6900 Cal yr BP for the Ebro delta (Sornoza et al., 1998), 6900 to 5100 Cal yr BP for the Pô delta (Amorosi et al., 2017), and 5000 Cal yr BP for the Tiber delta (Belotti et al., 1994). These temporal differences were likely controlled by the local climate, subsidence, and anthropic factors, which impacted significantly sediment transfer from different catchment areas.

On the geological time scale, we observe glacial and interglacial cycles that can be explained by external forcings. The main external forcings controlling the evolution of earth's climate correspond to the earth's orbital parameters and cycles (Milankovitch, 1941). During the Holocene, precession was the parameter that controlled the orbital insolation, with a cyclicity of 21700 years (Berger, 1977). In the Northern Hemisphere, summer insolation was at its maximum at the start of the Holocene (11700 Cal yr BP). Insolation has been decreasing since the middle of the Holocene, and a reversal was recorded 4500 years ago, with winter insolation becoming more important than summer insolation (Berger, 1978), reaching a maximum in the present-day (Berger and Loutre, 1991). Numerous

paleoenvironmental studies from temperate to tropical zones demonstrate the major forcing of this latest orbital change on terrestrial hydrological systems (Magny et al. 2012, Gasse et al. 2000).

Solar activity is also an external climate forcing that needs to be taken into account when addressing Holocene climate evolution. Numerous studies link variations in solar activity with climate change (Denton and Karlén, 1973; Bond et al., 1995; Magny et al., 2010). Phases of minimum solar activity are generally associated with phases of significant glacier advancement (Wiles et al., 2004), climate instability, and high erosion (Berger and Loutre, 1991).

Volcanic events are another external forcing to have an impact on climate. The release of particles into the atmosphere blocks part of the solar radiation leading to a drop in temperature. Depending on the type and size of the eruption, the temperature drop may be regional or global (Wagner and Zorita, 2005). Combined with minimum solar activity, this accentuated colder and more erosive events during the Little Ice Age (LIA) (Grove, 1988).

To assess the morphological evolution of deltas in response to recent artificialization of river systems and future climate change, we propose an approach based on the study of the sedimentary records of the Rhône delta as a representative deltaic system during the last glacial-interglacial Holocene transition, which evolution can be compared to well-studied Mediterranean deltas such as the Pô, the Ebro and the Nile deltas. The factors controlling the sedimentary variations through time, such as climate (Bond et al., 1995; Mayewski et al., 2004) and anthropogenic activities (Bravard et al., 1999; Liébault and Piegay, 2002; Vauclin et al., 2020), have been assessed through the study of the variations of the depositional environment through time, the changes in fluvial style in the watershed system, and the coastline displacement linked to the relative variations in sea level. In this study, we focus on the period ranging from the end of the last glacial period (beginning of Holocene, 11700 Cal yr BP) to the present day, where most of the factors controlling the evolution of the coupled watershed-delta system, such as sedimentary fluxes (Bravard et al., 1997), rainfall (Pichard, 2017), insolation (Berger and Loutre, 1991), land use (Berger et al., 2003), and dam sedimentary storage (Petts and Gurnell,

2005), can be quantified.

The Rhône river is located in the northwestern part of the Mediterranean (Fig. 1A) and its watershed extends over almost 100000km² and is subject to different types of climates: oceanic, Mediterranean, and mountainous. Moreover, the North Atlantic Oscillation mentioned above had a different impact on the hydrology of northern and southern parts of its watershed (Bladé et al., 2012). The onset of agricultural societies from 7800 years Cal yr BP is also well documented (Berger et al., 2016), and since the end of the Neolithic period these strongly modified the natural hydrological regime and sedimentary transport (Berger et al., 2016). A collective project has studied the hydrosedimentary functioning of the river (using robust instrumentation) since the start of short-circuiting in the mid-20th century, in partnership with the river's main managers (Provansal et al. 2014; OSR 1-6 project, Boudet et al. 2017). For these reasons, the Rhône, its catchment, and its delta have been studied for many years, and a wealth of data is therefore available. Finally, this delta is at risk from future climate change, and therefore presents strong economic (mainly agricultural) and ecological challenges. To understand its future evolution, the study of its past functioning and trajectory is essential. By improving the chrono-stratigraphic model, we will be able to calculate the volumes of sediment deposited in the Rhône delta and relate them to climatic and anthropic changes in the catchment.

2. Context

The development of the Rhône Delta is linked to the post-Quaternary history of the Gulf of Lions area, and its architecture is inherited from the Late Glacial Maximum (LGM) morphology. The initial step in its development was the Pyrenean orogeny that induced folds in the south, which were then reactivated during the Alpine compression (Guimera and Alvaro, 1990). During the Messinian salinity crisis that dried up the Mediterranean, the sudden lowering of the base level induced drastic canyon erosion of the underlying deposits. The Messinian canyons are located in the present-day shelf break in front of the Rhône delta and were filled by 1200 m of sediment during the Pleistocene (Clauzon et al., 1996). The Gulf of Lions platform is considered to have been tectonically stable since the Messinian

crisis (Lefebvre, 1980; Rabineau, 2005). During the LGM, the Petit Rhône and Grand Rhône paleo-canyons were eroded across the shelf break. At the scale of the western Mediterranean, the platforms corresponding to the present-day shelf are made up of stacked low stand prisms, enhanced by the fact that the periods of high level were very short during the Quaternary, with reduced or absent deposits (Chiocci et al., 1997) and possible removal by erosion during subsequent phases of sea-level fall. However, the continental shelf of the Gulf of Lions shows good preservation of regressive deposits, which were continuous in the axis of the Rhône channel during the Pleistocene (Gensous and Tesson, 2003).

The Rhône delta is a sedimentary system that started to enlarge during the Holocene (Arnaud-Fassetta and Provansal, 1993). Numerous stratigraphic studies (e.g., Arnaud-Fassetta, 1998; Vella et al., 2005; Jouet, 2007; Amorosi et al., 2013; Fanget, 2013; Arnaud-Fassetta and Suc, 2015) have defined a Holocene stratigraphic framework covering the region from the present-day deltaic plain and continental shelf towards the distal shelf break canyon. The Rhône watershed, which is subject to the same controlling factors described above, has also been studied for many years, permitting assessment of the dynamics of the hydrosystem over time. The morpho-sedimentary dynamics (e.g., Bravard et al., 1997; Arnaud-Fassetta, 1999; Arnaud et al., 2012; Salvador and Berger 2014), climatic variations (Magny, 2004; Holzhauser et al., 2005; Debret et al., 2010), and anthropogenic activity (e.g., Archaeomedes, 1998; Benoit et al., 2000; Guilaine and Manen, 2005; Berger et al., 2007; Notebaert and Berger, 2014; Berger et al., 2019) strongly influenced the hydrosedimentary activity of the watershed during the Holocene.

The present-day Rhône delta has a deltaic plain that extends over 1742 km². The apex of the delta is located in Arles, where the Rhône then separates into two arms, the Grand Rhône to the east and the Petit Rhône to the west (Fig. 1B). The shoreline is located between 30 and 45 km from the apex. The deltaic plain can be divided into three parts: the Petite Camargue to the west of the Petit Rhône, the Grand Camargue between the Petit and Grand Rhône, and the Grand Plan du Bourg to the east of the

Grand Rhône. The altitude of the deltaic plain does not exceed 5 m NGF (Nivellement Général de la France; the official levelling network in mainland France) and corresponds to the remains of the paleo coastline ridges or the fluvial levees (Arnaud-Fassetta et al., 2015). Most of the surface of the deltaic plain does not exceed 2 m NGF, which makes it sensitive to sea level variations.

The interglacial period started at the beginning of the Holocene (11700 Cal yr BP). It was initiated by a global warming that led to the decrease in the amount of ice at the poles and a phased rise in sea level from -120m masl at the LGM (Lambeck et al., 2002; Stanford et al., 2011), to -50m masl after a melt water pulse recorded at 11 300 Cal yr BP (Bard et al., 2010; Smith et al., 2011). This rapid sea level rise induced the retrogradation of Mediterranean deltaic system until 7000 Cal yr BP (Stanley, 1997; Labaune et al., 2005; Berné et al., 2007), which started to prograde from 7000 Cal yr BP onwards, due to the stabilization of the sea level close to its present-day level (Stanley and Warne, 1994).

The development of the Rhône delta is based on the successive progradation of different sedimentary lobes linked to the avulsion of different distributary channels on the deltaic plain after 7000 Cal yr BP. The main sedimentary lobes of the delta are the lobes of Saint-Ferréol, Ulmet, Peccaïs, Bras de Fer, and Roustan (Arnaud-Fassetta, 1998; Vella et al., 2005).

The Saint-Ferréol lobe is located in the median part of the deltaic plain (Fig. 1B). Its progradation started at 7000 Cal yr BP and ended in 1440 CE (Vella et al., 2005), following artificial closure of the distributary channel. It shows a pulsed growth with progradation phases synchronous with periods of hydrosedimentary abundance (Provansal et al., 2003). Dated barrier beaches permitted to quantify the rate of advance of the lobe during its progradation, that ranges from 1.5 m/year to 75 m/year (Vella et al., 2005). The phases of rapid progradation are the result of significant hydrological and erosive activity in the watershed, which induced intense sediment transport through the river systems. At the beginning, symmetrical growth prevailed with a fairly low progradation rate ($<50\,000\text{ m}^2/\text{yr}$) until 4800 Cal yr BP (Vella et al., 2008). An acceleration of the lobe progradation between 4800 and 2500 Cal yr BP is then recorded and is thought to be related to stabilization of the sea level (Provansal

et al., 2003). The first evidences of instability are recorded in Roman times (2200–2000 Cal yr BP), with avulsions occurring in the 2nd and 6th centuries AD, caused by an increase in sediment load carried by the fluvial system, causing a rapid progradation, and a concomitant rise in sea level (Arnaud-Fassetta 2002; Provansal et al., 2003).

The Ulmet lobe is located in the eastern part of the deltaic plain (Fig. 1B). Contemporaneous with the Saint-Ferréol lobe, its progradation started at 6500 Cal yr BP and ended in 1440 CE (Vella et al., 2005), after the artificial closure of the distributary channel. The geometry of the lobe is not precisely constrained because the nearshore paleochannels are poorly outcropping on the present-day deltaic plain. Despite its slower progradation, this lobe represents a significant volume of the prodeltaic sedimentation (Vella et al., 2008).

The Peccaïs lobe is located in the western part of the present-day deltaic plain (Fig. 1B). Its progradation started at 1950 Cal yr BP and ended in 1552 CE (Rey, 2006) with the setup of the Petit Rhône channel. The growth rates of the Peccaïs lobe are variable through time, and the sedimentation rates assessed for the Peccaïs lobe are higher than those of the Saint-Ferréol lobe (Vella et al., 2008). The Peccaïs lobe is asymmetric due to the avulsion of the “Grau Neuf” channel in the eastern part of the lobe, creating a secondary axis which prograded faster (Vella et al., 2005).

The Bras de Fer lobe is located in the eastern part of the present-day deltaic plain (Fig. 1B) and developed at the top of the Ulmet lobe. Its progradation started in 1587 AD during the Little Ice Age and ended in 1771 CE (Colomb et al., 1975; Rossiaud, 1994) with an artificial avulsion. This lobe shows a rapid progradation linked to a very high sediment supply, probably related to the frequent floods that were recorded during the Little Ice Age (Arnaud-Fassetta and Provansal, 1999; Provansal et al., 2003) coupled with low vegetation cover in the watershed, which induced a high soil erosion potential. The Bras de Fer lobe recorded its fastest progradation between 1665 and 1688, with an average rate of 160 m/year (Provansal et al., 2003). During the 16th century, the avulsion of the distributary channels on the Rhône delta plain was controlled by human activity (Colomb et al., 1975).

The most recent part of the Rhône delta sedimentation is the present-day mouth of the Grand Rhône channel corresponding to the Roustan lobe (Fig. 1B). Artificially developed from 1711 CE onwards, the termination of the Grand Rhône channels was divided into three distributary channels: Piémanson, Roustan, and Pégoulie (from East to West). In 1885 CE, two distributary channels were closed and only the Pégoulie distributary channel was left active, for navigational reasons (Provansal et al., 2003). Since 1860 CE, the mouth of the Grand Rhône channel has been artificially fixed (Maillet et al., 2006). During a period of increase of the sediment supply (1895-1952 CE), the coastline of the Grand Rhône had a progradation rate of 60 m/year (Vella et al., 2005). In 1892, the Roustan distributary channel was reopened to facilitate navigation while the abandoned Pégoulie channel naturally filled up with sediment. Since this date, the Roustan distributary channel has been the only active branch of the Grand Rhône.

The sedimentary dynamic of the Rhône delta is also directly influenced by the interaction between waves and the river dynamic (Sabatier et al., 2001). The waves reach their maximum speed in the levigation zone (the deepest area between beaches), i.e., in front of the present-day beaches in the western part of the present-day Rhône river mouth. This levigation zone is characterized by low sediment load but high erosion potential (Maillet et al., 2006a).

Even if it is known that wave action has an impact on the development of the Rhône delta (Sabatier et al., 2009) by reshaping its front and redistributing the sediment away from the river mouth, the architecture of the Rhône delta is mainly influenced by the long-term river dynamics.

Indeed, the development of this microtidal delta (Maillet, 2005) over time is controlled by the avulsions of the main distributary channels, as well as by the variations in hydrological flow and sediment load carried by the river through time. The Rhône river has experienced phases of very high hydrosedimentary activity, notably during the Little Ice Age (the 15th to 17th centuries) (Pichard et al., 2014), coeval with the rapid development of the Bras de Fer lobe (Provansal et al., 2005; Vella et al., 2005). The sediments deposited in the delta are mainly supplied during floods (Maillet et al., 2006),

which intensity and frequency increased during the Little Ice Age, favored by advances of major glaciers in the northern Alps and higher hydrosedimentary connectivity at the catchment scale (Bravard, 2010; Debret et al., 2010, Pichard et al., 2014).

3. Materials and Methods

3.1. Sedimentary core data

Seventeen cores collected during several research campaigns (Table 1) in the present-day delta plain and in the prodelta were subjected to sedimentological analysis and were sampled for dating (see locations on Fig. 1B). Three cores were collected by the INRAP rescue Archeology Institute in the apex of the delta (Arles city area, Fig. 1B) (cores GMSC1, GMSC1A, and GMSC8). In the deltaic plain, five cores were collected by the PEH project "Vallée du Rhône" and the ANR Armilit and Eurodelta programs (cores FG, SF, FP3, R1 and R2). In the prodelta, nine cores collected by IFREMER in various campaigns were studied: RHS-KS04, RHS-KS21, RHS-KS27, RHS-KS40, RHS-KS51, RHS-KS55, and RHS-KS57, collected during the Rhosos campaign of IFREMER, BMKS21 collected by the Beachmed program of IFREMER, and MD99-2352 collected by IFREMER.

3.2. Sedimentological analysis

The seventeen cores have been analyzed in order to reconstruct the paleoenvironmental characteristics of each core, based on sedimentological analysis. The sedimentological analysis consists of the description of each core in terms of grain size vertical evolution, sedimentary structures, bioturbations, color, accessory material such as shells, bioclasts, plant debris and microcharcoal fragments. The sedimentological analysis enables to classify several sedimentary facies according to their genesis in terms of processes of deposition that characterize specific depositional environments. Remarkable stratigraphic surfaces such as Maximum Regressive Surfaces (MRS) and Maximum Flooding Surfaces (MFS) were also identified on each core and were used together with the facies analysis to define transgressive and regressive cycles (T/R cycles). The T/R cycles were correlated between the cores following North-South and West-East transects.

3.3. Chronostratigraphy

Improvement of the chronostratigraphic model to enable accurate estimation of the temporal volume of sediment deposited in the deltaic system is key part of this study. A total of 92 dates were realized during past studies (Vella, 2005; 2008; Berné et al., 2007; Amorosi et al., 2013; Vella and Sivan, 2014; Fanget et al., 2014), and these have helped to constrain the chronostratigraphic scheme of the delta. In this study, 95 new radiocarbon dates were performed to complete the existing dataset and to better constrain, stratigraphically and geographically, the evolution of the deltaic system (See supplementary data).

The chronological framework was completed by radiocarbon dates on charcoal and marine gastropods, bivalves and foraminifera shells (See supplementary data table for details). Charcoal and marine shells were extracted from the sediment using a sieving methodology that consists in pouring a dilute aqueous solution of sodium hexametaphosphate over the samples to facilitate the recovery of dateable materials favouring charcoal and floatwood micro-debris and secondarily coarse shell in a living position at best. The samples were sent to the Poznan Radiocarbon Laboratory for ^{14}C AMS datings, because of the low carbon quantities in the samples. Wood and charcoal samples were systematically favored over marine shells to prevent from reservoir effects. The uncertainty in the age calculation varies between 20 and 200 years, depending on the quality of the samples and the quantity of carbon. The calibrated age of charcoal was calculated using Calib version 8.20 with the IntCal 20 calibration curve (Reimer et al., 2020). The ages of marine shells were calculated using Calib 8.20 with the Marine20 calibration curve (Heaton et al., 2020). For calibration of ages from marine shells, the local reservoir correction was computed by using <http://calib.org/marine/>. The reservoir correction computed is $\Delta R = -171 \pm 77$ yr.

3.4. Calculation of sediment volume

The estimation of the sediment volumes deposited in the Rhône delta during the Holocene is one of the main contributions of this study. The volume calculation was performed on the basis of the

stratigraphic correlations. The study area used for the calculation is a square mesh of 92 km encompassing the whole Rhône delta system divided into 2-km-long cells (Fig. 1B). This dimension allows the delta to be covered from the apex down to the canyons located at the shelf break, including the area of resedimented particles on the sides of the present-day delta shoreline. The method chosen for the calculation evaluates the difference in thickness between the present-day topography and that estimated for 12500 Cal yr BP. The difference gives the thickness of the sediment deposited for each cell in the mesh. The values of all cells are then summed to obtain the global volume of stored alluvial material. The present-day topographic surface of the whole delta was obtained by concatenating the data of the submerged part and the ones of the emerged part of the delta. For the submerged part, the data were made available by IFREMER, with the bathymetric surface data being obtained through oceanic cruises with multibeam echosounders, scanning sonars, and seismic data (Berné et al., 2007). These technologies enabled to obtain a resolution of about 100 m over the entire Gulf of Lions. For the emerged part, the topography was obtained from digital terrain models. These models were generated from the geoprocessing of satellite images, and the resolution used for this study was 100 m. The reconstruction of the 12500 Cal yr BP topographic map was made based upon subsurface data. In the north, for the present-day deltaic plain, the 12500 Cal yr BP surface was updated using the sedimentary cores of this study and the BSS database of BRGM (<https://infoterre.brgm.fr/page/banque-sol-bss>), with a total of 59 control points being used to improve the surface created in previous studies (Vella et al., 2005; Arnaud-Fassetto and Suc, 2015). The northeastern part and the northwestern part of the study area are outside of the deltaic plain and were not included in the estimation of the sediment volume deposited. For the central and southern parts of the study area, the map proposed by Jouet (2007) was used. This map is a reconstruction of the surface at 20 000 Cal yr BP, corresponding to the erosion surface of the LGM. This map was constrained by the interpretations of the seismic profiles of the Gulf of Lions (Jouet, 2007; Fanget et al., 2014). To estimate the difference in topography between the 20 000 Cal yr BP surface (Jouet, 2007) and our 11 700 Cal yr BP surface, isopach maps of different units identified in the prodelta were used (Labaune et al., 2005). These isopach maps cover a large part

of the prodeltaic system. The last part of the 11 700 Cal yr BP topographic map is a band of 6 km to the east and west in the prodelta that is not present in the 20 000 Cal yr BP surface (Jouet, 2007). To complete each side of the new map, the trend in the difference between the present-day topography and 11 700 Cal yr BP was calculated inside the 20 000 Cal yr BP and interpolated to each side. This 11 700 Cal yr BP surface included data produced in a previous study on the delta system (Labaune et al., 2005; Vella et al., 2005, Jouet, 2007; Arnaud-Fassetta and Suc, 2015).

3.5. Sediment compaction estimation

In delta systems, sediment compaction has an important role in short term subsidence (Stefani and Vincenzi, 2005; Van Asselen et al., 2009). This subsidence can be of tectonic and lithospheric origin at the scale of several million years, although at shorter time scales, subsidence can be related to human activity involving extraction of water or hydrocarbons from the subsurface (Teatini et al., 2010), or the natural phenomenon of porosity reduction through pressure caused by the burial of deposits.

In the case of the Rhône delta system in the Holocene, the observed subsidence is related to the compaction of sediments. As it is difficult to compute the exact compaction due to sediment loading, which depends on water saturation, sediment density, and the types of particles, it is necessary to simplify the computation by assuming that the present-day deltaic plain and its underlying deposits correspond to 65% sand and 35% clay, percentages based on estimates calibrated with the core descriptions and the correlation transects made across the delta. Compaction estimates were made considering the two main lithologies observed in the Rhône delta.

4. Sedimentary analysis and delta architecture

4.1. Facies associations (FA) analysis

The Rhône delta is characterized by clastic sedimentation, with the particles originating from the Rhône watershed (Fig. 1B). The various depositional environments are present along a depositional

profile ranging from the present-day deltaic plain to the prodelta at the entrance to the plateau-edge paleocanyons. The facies associations are summarized in Fig. 2. Eight Facies Associations have been defined based on the sedimentological analysis of the seventeen cores and are presented hereafter in stratigraphically proximal to distal order.

4.1.1. The fluvial channel facies association (C1)

This facies association is composed of coarse to very coarse-grained, very poorly sorted sand, with rare granules and gravels and occasional cross-stratification at mega-ripples scales. The base of this facies association is erosive and is organized into fining upwards sequences from coarse grained sands up to fine grained sands to silts, the thickness of which can reach 4 m (R2 core). This facies association is well developed in the early Holocene strata of cores located near the present-day shoreline (R1, R2 and SF cores), and constitutes the main sedimentary record close to the apex of the delta (cores GMSC1, GMS1A, and GMSC8).

4.1.2. The fluvial plain facies association (C2)

This facies association shows brownish to reddish horizontal plane-parallel silty clays deposits including decimeter thick rippled very fine to fine-grained non-erosive sand beds. The silty clays indicate lower flow regime that allowed for suspension fall out in backwater during channel abandonment (Smith et al., 1989). The sands are interpreted as channel overbank or crevasse-splay deposits (Allen, 1963, 1965; Miall, 1996;). This facies association is present in the upper part of the deltaic plain core (R1, R2, SF, FG, FP3), or in alternation with C1 in the apex core (GMSC1, GMS1A, GMSC8).

4.1.3. The bay facies associations (B1 and B2)

The bay Facies Associations have subdivided into Inner Bay Facies Association (B1) and outer Bay Facies Association B2, as shown on Fig. 2. These facies association is made up of bioturbated clay to silty clays alternating with centimetric lenses of sands including microfossils. Locally, sand beds show thin fining upward muddy sands with scattered medium to coarse grains including faunal accumulation and

abundant plants debris and mudclasts. This muddy-dominated environment indicates suspension decantation in a quiet deposition environment. Fauna-rich fine-grained sandstone beds are interpreted as storm deposits. This facies association is present in the lower and upper parts of the cores located in the present-day deltaic plain (R1, R2, SF, and FG cores).

4.1.4. The mouth bar facies association (MB)

The mouth bar facies association shows bioturbated fine to coarse-grained sands, moderately sorted with abundant clay pebbles. This association is organized into coarsening upwards and thickening upwards sequences, with traction structures due to ripple migration. This Facies Association typically occurs in cores FG, SF, and R2 cores, often in association with bay deposits (B1 Facies Association).

4.1.5. The upper delta front facies association (U1)

The upper delta front association shows sharp-based coarsening and thickening upward fine to coarse moderately sorted sands, moderately bioturbated, with abundant plant debris. This facies association is 0.5 to 2 m thick and contains dispersed gastropods. Trough cross bedding, tangential oblique and plane parallel bedding are common. Some clay levels of 5 to 10 cm thickness are observed on the bottom of the facies association but are missing upwards. The sedimentary structures and plant debris indicate overall progradation of the delta front fed by hyperpycnal flows and bedload processes (Elliott, 1976, 1986; Bhattacharya and Mac Eachern, 2006; Olivero et al., 2008), and the system is described as a flood-dominated river-deltaic system by Mutti et al. (2000). The scarce preservation of fine-grained sediments indicates a high-energy regime due to the fair-weather wave activity.

4.1.6. The lower delta front facies association (D2)

The lower delta front facies association is made up of alternating very fine-grained bioturbated silty sands with decimeter-thick beds of fine to medium grained sands. Bioturbation is more abundant than for the D1 association, and the sequential organization corresponds to coarsening upwards and thickening upwards stacked bedsets. Sedimentary structures denote the interplay between storm

waves that reworked the particles and forming hummocky cross-stratification-like sedimentary structures, and traction currents due to discharge, that formed low energy tractive sedimentary structures such as current ripples. This FA generally forms plurimetric intervals at the bottom of the upper delta front association and corresponds to the bottom of the delta front progradation.

4.1.7. The prodelta facies association (M1)

The prodelta association consists of coarsening and thickening upward highly bioturbated massive poorly sorted grey muddy siltstone alternating with medium-grained sands including shell fragments. Current ripples are observed in the fine-grained facies. This facies association was burrowed by *Skolithos* and *Ophiomorpha*. These deposits are interpreted as suspension settling from sediment-laden hyperpycnal flows of hemipelagic plumes (Orton and Reading, 1993) or pycnocline processes created by internal waves (Mateu-Vicens et al., 2012) in a prodeltaic open marine environment below the fair-weather wave base level.

4.1.8. The offshore facies association (M2)

The offshore facies association is dominated by clayey facies. *Skolithos*, *Planolites*, *Cruziana*, and *Ophiomorpha* ichnofacies are recognizable. These clayey facies also present some occurrences of thin bioturbated bioclastic fine-grained sands with reworked shell debris. This facies association is interpreted as suspension fall-out in an upper offshore environment (20 to 60 m water depth), occasionally submitted to storm processes below the fair-weather wave base (Dott and Bourgeois, 1982). Thick intervals of clayey facies with the absence of hydrodynamic sedimentary structure and sands suggest very low energy conditions in a lower offshore environment below storm waves.

4.2. Sedimentary logs and facies stacking

To illustrate the diversity of sedimentary assemblages observed in the Rhône delta, three reference cores were selected because of their diversity of facies associations and stacking, as well as the sequential organization of the deposits. Core GMSC1A represented the delta apex, core FG is located

in the deltaic plain, and core MD99-2352 is located in the prodelta (Fig. 3). The sequential organization was defined following the transgressive/regressive cycles defined by Van Wagoner et al. (1988) and Embry (2002, 2009a, 2009b), although on a different scale. The high-frequency depositional cycles illustrated below are bounded by flooding surfaces (parasequences) in the marine successions or by erosional/hiatal surfaces within continental deposits.

4.2.1. Core GMSC1

The GMSC1 core is located in the apex of the delta (Fig. 1B), on the western bank of the Rhône River in the city of Arles. This core is 24.30 m long and has been divided into five cycles based on sedimentological characteristics and the evolution of vertical facies stacking. Five datings on charcoal fragments indicate a sedimentary record that ranges between 2744 Cal yr BP (bottommost datings) to 1937 Cal yr BP (topmost dating), covering the Iron Age and High Roman Empire periods. The first cycle at the bottom of the core (from 24.30 to 15.90 m), corresponds to medium to coarse-grained sands organized in multi-decimeter to meter-thick fining upwards sequences, with trough cross-bedding stratifications and current ripples on top of the bedsets, passing upwards into decimeter-thick beds of clayey-silt to medium-grained sand, organized into coarsening upwards sequences. This cycle is composed of stacked fluvial channels (facies association C1) filling a fluvial valley preserved during base level rise in a transgressive trend, followed by channel overflow deposits, and belongs to the alluvial plain facies association (C2).

A second cycle (from 15.90 to 6.10 m), comparable to the first one, is made up of multi-decimeter thick fining upward bedsets of coarse to fine-grained sands with plane parallel lamination, trough cross stratifications, and current ripples, passing upwards to clayey-silts with abundant ceramic fragments from the Roman period (Vella et al., 2014) associated with waste that testifies to the presence of continuous human occupation. This cycle records stacked fluvial channel fill deposits preserved in a transgressive trend, overlaid by anthropogenic soil that developed in a floodplain environment (C2 facies association).

This interval is overlain by a thin package of thin-bedded fine to medium grained sands with current ripples, on top of which sit silty clayey deposits, on top of which ceramic fragment-rich clayey silts are preserved (8.50 to 6.60 m). It corresponds to a short cycle of floodplain deposit preservation, with river overbank deposits overlaid by anthropogenic cumulic soil.

Above this, a near identical cycle ranging from 6.60 to 1.9 m records floodplain aggradation with river overbank clay and silt deposits overlaid by a thick (3.6 m) interval of ceramic-rich anthropogenic cumulic soil.

A last cycle on the top of the core (1.9 to 0 m) corresponds to coarse to medium-grained sands organized in fining upwards bedsets with floating granules and ceramic fragments. It is interpreted as fluvial channel fill and records the last avulsion of the river at this location.

This core illustrates the Rhône fluvial channel avulsion events that occurred in the apex of the delta plain, with human occupation on the riverbanks when the active channel shifted.

The radiocarbon dates realized during this study (Appendix A) allow the stratigraphic cycles to be chronologically constrained.

4.2.2. Core FG

Core FG is located in the present-day deltaic plain, in the southwest of the Vaccares lagoon (Fig. 1B). The core is 42.10 m long and is subdivided into seven cycles recording transgressive/regressive trends bounded by remarkable stratigraphic surfaces (e.g., Maximum Regressive Surfaces) that can be correlated with other cores of the Rhône delta system (see next section). The radiocarbon dates realized during this study (Table 1) allow the stratigraphic cycles to be chronologically constrained. Sixteen radiocarbon dates were acquired, but only 13 were retained for stratigraphic correlations. The bottom of the core is made up of gravels forming the "Cailloutis" that corresponds to the substrate for the overlying Holocene succession and is suggested as representing a late Pleistocene fluvial-channel deposit formed during the LGM (Amorosi et al., 2013).

Above the Cailloutis, the first cycle (40.80 to 32.20 m) corresponds to the Holocene transgression and drowning of the LGM alluvial plain (Oomkens, 1970; Amorosi et al., 2013). The Cailloutis is made up of coarse-grained sands with floating granules in a silty clayey matrix at the base, passing upwards to bioturbated silty mud with occasional lenses of medium-grained sands with current ripples and organic-rich shaly intervals (dated from $10\,935 \pm 50$ Cal yr BP, see Fig. 3). Above this interval, a several-meter thick package of silty clays, moderately bioturbated with shell fragments and foraminifera, passes upwards to an alternation of silts with centimetric lenses of medium grained bioturbated sands with current ripples and HCS-like bedforms. This cycle records deepening-upward trend above the Cailloutis, starting with a transgressive lag, on top of which bay environments were preserved (as also described by Amorosi et al. (2013) for two cores [R1 and R2] located close to this FG core), recording the onset of the Holocene transgression. A marine flooding surface was identified on top of the coastal environment, with the sedimentation of marine silt/mud showing open marine fauna (foraminiferal assemblages composed of *Elphidium macerium*, *Quinqueloculina seminula* and *A. beccarii* forma *inflata*, as described by Amorosi et al., 2013 in the same sequences in cores R1 and R2) typical of the open marine environments. The progressive occurrence of rippled sand lenses records the progressive progradation of the system with prodeltaic deposits. This regressive interval records the first occurrence of the Rhône delta progradation around 6800–6000 Cal yr BP.

Above this cycle, a second interval (32.20 to 25.50 m) corresponding to bioturbated silty mud with occasional rippled medium-grained sand packages passes progressively upwards to coarsening upwards fine to medium-grained sands showing contorted and slump structures. This interval records a second phase of progradation of the delta system, dated between 6000 and 4700 Cal yr BP (Fig. 3), with offshore to prodeltaic environments at the base of the cycle, passing upwards to slumped delta front bottom sets (distal delta front).

A third interval ranging from 25.50 to 17.00 m is made up of bioturbated silty clays alternating with centimeter to decimeter-thick rippled fine to medium sand lenses organized in coarsening upwards

bedsets. This interval is organized into two cycles of coarsening upwards and thickening upwards sequences recording pulses of progradation of the delta (Ulmet lobe), with prodeltaic facies passing progressively upwards to a distal sandy delta front, in a period ranging from post 4700 to 3000 Cal yr BP.

This interval is followed by another cycle (17 to 11 m) composed of silty mud with abundant centimeter-thick medium-grained lenses of sands showing current ripples and burrows, passing progressively upwards to multi-decimeter-thick sets of coarsening upwards and thickening upwards medium to coarse-grained moderately-sorted clean sands with plane parallel and oblique structures, with occasional mud pebbles and granules, bioturbated on top. This cycle is interpreted as the progradation of the delta front system on top of the prodeltaic and lower delta front environments. This records an important phase of the delta progradation of the Ulmet lobe, dated to around 1660 Cal yr BP.

A following sequence from 11 to 3.8 m is made up of multi-decimeter-thick beds of fine to medium-grained sands with oblique lamination, passing upwards to medium to coarse-grained sands with oblique lamination to 3D megaripples. This interval is interpreted as a prograding upper delta front system, recording the most recent progradation phase of the Ulmet lobe system that ended around 1000 Cal yr BP (Fig. 3).

This interval is capped by reddish silty mud (3.8 to 1.5 m) that correspond to the recent fluvial channels preserved on top of the progradation. The topmost part of the core (1,5 to 0 m) has not been recovered.

4.2.3. Core MD99-2352

This core is located in the present-day prodelta, 27 km from the coastline (Fig. 1B). The six new radiocarbon dates realized during this study (Table 1) allow us to chronologically constrain the sedimentary cycles. The oldest radiocarbon dates yielded an age of 15120 Cal yr BP (Berné et al., 2007)

at a depth of 14.9 m (Fig. 3). Other dates indicate that the Holocene is only included in the last 3 m of the core. The high pre-Holocene sedimentation rate is the result of the proto-Rhône delta development (Early Rhône Deltaic Complex - ERDC). The prodeltaic sediments deposited between 2.2 m and 15.1 m correspond to the distal part of the ERDC (Berné et al., 2007). The ERDC was initiated during the Younger Dryas, which corresponds to a cooler period during the post LGM global warming. The Younger Dryas corresponds to a period of decreased sea-level rise and increased sediment flux (Berné et al., 2007).

The bottom of the core (15.40 to 15.05 m) is made up of coarse to very coarse-grained sands, interpreted as fluvial deposits (C1), and corresponding to the post glacial substratum for the Rhône delta development (Berné et al., 2007).

Above the basal "Cailloutis" lays an interval (15 to 10.0 m) of bioturbated mud with occasional shells and foraminifers, on top of which lay centimeter to decimeter-thick medium to coarse-grained sandy beds with current ripples. These are interpreted as offshore marine deposits capped by prodeltaic deposits, forming a first marine progradation trend on top of the substrate. This prograding unit is dated from 15 000 to 13 000 Cal yr BP and corresponds to the first transgressive-regressive cycle of the Rhône delta recorded in the distal part of the system.

This interval is overlaid by a thick package (10.8 to 3.5 m) of mud with occasional centimetric fine-grained sand lenses, sometimes showing HCS-like bedforms, ending up with decimetric coarsening-upwards structureless fine to medium-grained sands. This interval is also interpreted as offshore deposits capped by prodeltaic deposits, recording a second phase of progradation of the deltaic system in the distal part, dated to between around 13 000 and 12 000 Cal yr BP.

A third sequence (3.5 to 2.1 m) made up of several decimeter-thick coarsening-upwards sequences of silty mud capped by fine to medium-grained sands showing faint current ripples is also interpreted as a small prograding package from offshore to prodeltaic settings.

Above, a thin sequence of coarsening upwards mud to fine to medium grained bioturbated sands (2.1 to 1.3 m) records a prograding package of offshore to prodeltaic deposits.

The topmost part of the core (1.3 to 0 m) represents a cycle based on an erosional surface on top of which a several decimeter-thick fining upwards coarse to fine-grained sand showing megaripples passes rapidly upwards into bioturbated silty clays with abundant shell fragments. The sandy package can be interpreted as a high-density flow event derived from fluvial input (flood event), on top of which offshore sedimentation occurred. This interval is dated between 4075 and 949 Cal yr BP and corresponds to the last dating on the top of the core, revealing a very low Late Holocene sedimentation rate in this area.

During the rapid marine transgression, a small amount of sediments were deposited in this area, with only 1.1 m in 6500 years. Since the stabilization of the sea level at 6000 Cal yr BP (Vella et al., 2008), 1.5 m of sediment has been deposited. A sandy pulse was present between 5500 and 4100 Cal yr BP and may be contemporary with the development of the Saint-Ferréol and Ulmet lobes during this period (Arnaud-Fassetta and Suc, 2015)

4.3. Stratigraphic architecture of the Rhône delta

FA analysis and stacking of the cores available for the Rhône deltaic system enabled us to identify correlatable surfaces (mainly maximum regressive surfaces) constrained by age (as defined in Table 1), and to propose correlation transects highlighting the stratigraphic architecture of the Rhône delta. Three main correlation transects were made across the delta (Figs 4, 5, 6 and 7; see location of the transects in Fig. 1B), and six main sequences were identified for the Holocene period, starting on top of the Cailloutis that corresponds to the Plio-Pleistocene glacially-derived conglomerates (Griolet, 1976), and ending at the present-day surface.

4.3.1. Sequence 1 (11 700-4300 Cal yr BP)

Sequence 1 is bounded at the bottom by the top of the Plio-Pleistocene Cailloutis, which corresponds

to the Durancian fans that developed during the Wurm period, and thus forms the substrate for Rhône delta system that developed during the Holocene. Above the top Cailloutis surface, the age of which is assigned to 11 700 Cal yr BP, a several-meter-thick package of bay and mouth-bar deposits was identified in the R1 core (Transect 1, Fig. 4), FG core (Transects 2/3, Fig. 5), and R2 and SF cores (Transect 3, Fig. 6). This is interpreted as being deposited in the early Rhône deltaic plain and preserved in a transgressive trend that corresponds to the post LGM/early Holocene transgression. This interval is sharply overlain by offshore mud that highlight a rapid sea-level rise that occurred at 7500 Cal yr BP (Labaune, 2005) in the center of the present-day deltaic plain, passing to shallow marine and alluvial facies towards the proximal part of the system (the present-day apex of the delta). The maximum Flooding surface is dated 7000 Cal yr BP and marks the onset of the Rhône delta progradation. The offshore interval passes progressively upwards to prodelta and lower delta front facies associations in the axis of the present-day delta (core FG), testifying to a first pulse of delta progradation (early Ulmet lobe) that ended at the estimated date of 4700 Cal yr BP, and is characterized by a sharp surface on top of lower delta front sand in the FG core, interpreted as a maximum regressive surface.

4.3.2. Sequence 2 (4300-3000 Cal yr BP)

Sequence 2 is bounded at the base by the 4300 Cal yr BP maximum regressive surface corresponding to the top of the Sequence 1 regressive hemicycle and is well developed in the center of the present-day delta plain. This sequence corresponds to a major phase of delta front progradation that is well recorded in the R1 (Transect 1, Fig. 4) and SF and FG cores (Transect 3, Fig. 6), with a basal transgressive hemicycle very poorly developed. This regressive sequence corresponds to major phases of progradation of both the Ulmet and St Ferréol lobes that developed in the axis of the present-day delta. This sequence can be subdivided into two shorter-term progradational sequences that correspond to two minor pulses of progradation of both the Ulmet and St Ferréol lobes, thinning and passing southwards to prodeltaic and offshore sediments (KS04 and MD99 cores in Transect 1, KS40 core in Transect 2, and SG, 114, KS27, and KS51 cores in Transect 3). Sequence 2 is topped by a major

maximum regressive surface that corresponds to a sharp surface on top of coarse-grained delta front sands in the axis of the present-day delta.

4.3.3. Sequence 3 (3000-2000 Cal yr BP)

Sequence 3 is closely comparable to sequence 2 and is well developed in the central part of the present-day delta. In the proximal part of the system, this sequence corresponds to fluvial valley fill, as observed in core SC1 (Transect 2, Fig. 5). This passes distally to a shallow marine delta front system in the central part that records an important advance of the Ulmet and St Ferréol lobes in the axis of the present-day delta, and which shows mainly coarse-grained upper-delta front facies associations in the R1 (Transect 1) and R2, SF, and FG cores (Transect 3), thinning and passing distally to the south in prodeltaic and offshore deposits. This sequence corresponds to the maximum progradation of the Ulmet and St Ferréol lobes in the axis of the delta, which occurred until a major maximum regressive surface dated 2000 Cal yr BP, after which the St Ferréol lobe became inactive.

4.3.4. Sequence 4 (2000-1000 Cal yr BP)

Sequence 4 developed in the western and eastern parts of the present-day delta, in reaction to the Ulmet and St Ferréol lobes that prograded in the axis of the delta, forming a positive topographic relief, the highest point of which is reached in the axis of the SF core, seen at 1 m below the present-day surface. To the west, sequence 4 records the progradation of the Peccaïs lobe with a thick delta front facies association observed in the FP3 core (Transect 3). In the center part of the system, sequence 3 corresponds to the last phase of the Ulmet lobe progradation observed in the FG core (Transect 1 and 3). To the east, sequence 3 records the onset of the Bras de Fer/Grand Passon lobe progradation with delta front facies associations observed on the FG and SG cores (Transect 3), passing to the south into prodeltaic and offshore deposits (Transect 3, Fig. 6). The top of the sequence 3 progradation is characterized by a major maximum regressive surface corresponding to a subaerial erosional surface on top of which lie continental deposits of sequence 5.

4.3.5. Sequence 5 (1000-300 Cal yr BP)

Sequence 5 developed only on the western and eastern parts of the delta. This sequence is associated with the last stages of the Peccaïs lobe development to the west and the Bras de Fer lobe progradation to the east. The main facies associations observed in this sequence mainly correspond to delta plain deposits (i.e., alluvial, fluvial, and bay facies associations) in the proximal part of the system. These facies associations pass distally to well-developed delta front systems to the west (as observed in the FP3 core [Transect 1, Fig. 4] for the Peccaïs lobe), and rapidly to offshore deposits to the south. The Bras de Fer delta front system develops to the east and passes distally to offshore deposits to the southeast (Transects 2 and 3, Figs 5 and 6). Sequence 3 is capped by a maximum regressive surface estimated at 300 Cal yr BP.

4.3.6. Sequence 6 (300 Cal yr BP to present)

Sequence 6 is the last sequence recorded in the Rhône delta system and corresponds to the delta plain as it is observed today, with the still active Roustan lobe that has developed in the southeastern part of the system since 300 Cal yr BP (Transect 4, Fig. 6).

4.4. Estimated sediment volumes

4.4.1. Overall volume sedimented

The total volume sedimented computed by the difference between the 12500 Cal yr BP restored delta topography (Fig. 8) and the present-day delta surface resulted in an estimate of $89,7 \cdot 10^9 \text{ m}^3$ of sediment deposited over the last 12 500 years, taking sediment compaction into account.

The compaction has been estimated for the different classes of sediments. The sands have an initial porosity of 49% (Gustavs, 1992), and according to their compactness constant and the porosity evolution equation from Schmedemann et al. (2008), a sedimentary column of 40 m composed of sands measures 40.2 m when decompacted. The clays have an initial porosity of 82% (Dietrich, 1989), and according to their compactness constant and the porosity evolution equation (Schmedemann et

al., 2008), a sedimentary column of 40 m composed of clays measures 60.7 m when decompacted. Considering that clays are mostly present in the prodeltaic part, the phenomenon of compaction has mainly affected this zone.

Some uncertainties in the volume computation are due to the fact that a certain fraction of the sediments have been deposited out of the study area.

It is known that a certain volume of sediment was not deposited in the area used for the computation, as it by-passed the area and was deposited downstream in the deep sea system or was reworked by the long-shore currents (e.g., the Liguro-Provençal current and re-sedimented in long-shore drifts in the western part of the Gulf of Lions (Got and Aloïsi, 1990)).

Past studies evaluated that thirty percent of the fine-grained particles (e.g., clays and silts) that are supplied by the Rhône River are evacuated either towards the canyons of the Grand Rhône and Petit Rhône, or to the west into the Gulf of Lions (Got and Aloïsi, 1990). According to our results, 30% of the export corresponds to a volume of $17,7 \cdot 10^8 \text{ m}^3$. 1/6 of this volume, corresponding to $3 \cdot 10^9 \text{ m}^3$, is exported through the canyons of the Grand Rhône and Petit Rhône (Palanques et al., 2006).

The remaining part ($14,7 \cdot 10^9 \text{ m}^3$) is drifted to the west on the continental platform of the Gulf of Lions. The deposits in this area represent 1/7 of the volume deposited in the axis of the Rhône delta (Got and Aloïsi, 1989). In this study, the volume in the western part was estimated at $6,6 \cdot 10^8 \text{ m}^3$. The canyons to the west export the remaining $8,1 \cdot 10^8 \text{ m}^3$.

4.4.2. From volume to mass

Several decisions were made when transforming the volume of decompacted sediment (in m^3) into sediment mass (in tons). The first was to calculate only the solid mass, with the porosity of the sediment considered to be zero. The second decision, as for the previous steps, was to divide the sediments into two classes, clays and sands.

For the density calculations (Fig. 4C), sands were considered to have a density of 2630 kg/m^3 and clays an average density of 2750 kg/m^3 (Sharma, 1997). The initial porosity of sands is 49% and that of clays is 82%. Therefore, taking into account the porosity in the bulk density computation, the final whole densities are 1341 kg/m^3 for the sandy packages and 495 kg/m^3 for the clay packages.

Some generalizations were made to simplify the calculations in view of the accuracy of the data. To summarize:

- The present-day deltaic part (deltaic plain + delta front) represents 60.10^9 m^3 , and with 65% sand and 35% clay the total mass is $65.8.10^9$ tons.
- In the prodeltaic part, $48.4.10^8 \text{ m}^3$ with 20% sand and 80% clay corresponds to $39.4.10^9$ tons deposited.
- The deltaic system (deltaic plain, delta front, prodelta) of the Rhône has received a total of $105.2.10^9$ tons of sediments from the river.

The precision of the exports varies by 10% (Got and Aloïsi, 1990), and this uncertainty should be applied to the whole result, thus, between 95.10^9 and 115.10^9 tons of sediments were received over the last 11 700 years. Flow variations during the Holocene and their origins will be addressed in the Discussion.

5. Discussion

5.1. Rhône delta development calendar

5.1.1. From 11 700 to 7000 Cal yr BP

The first period considered in this study spans from 11 700 Cal yr BP to 7000 Cal yr BP and corresponds to the early transgression of the coastal deposits on top of the Pleistocene Cailloutis Fm. observed in the cores. This period is typically observed in Late Pleistocene-early Holocene incised valley fills worldwide (see inner bay, outer bay and bay-head delta deposits in Figs. 4 and 6), prior to the maximum marine incursion landward (corresponding to the main maximum flooding surface as

highlighted on the correlation transects, Figs. 4 to 7). According to the sedimentary record analysis, most of the deposits occur beneath the modern deltaic plain (Labaune et al., 2005; Berné et al., 2007; Jouet et al., 2007). This system is correlative in the distal deltaic system with the early Rhône deltaic complex that developed during a slowing down of the sea level rise occurring around 9000 Cal yr BP (Berné et al., 2007). Two avulsion phases of the paleochannel towards the northwest were highlighted (Berné et al., 2007), resulting in the migration of the lobes. The resumption of sea level rise eroded the topmost part of the early Rhône deltaic complex deposits (Bassetti et al., 2006) and the maximum flooding surface (MFS) was reached around 7000 Cal yr BP (Vella et al., 2005), with offshore deposits on top of the early Rhône deltaic complex coastal deposits.

The calculation of volumes for this period is made difficult due to uncertainties with horizon picking on seismic data because of the presence of gases that stopped the propagation of seismic waves and the small amount of sedimentary data (Aloisi et al., 1975; Enget et al., 2014). However, according to our calculation method, 21, 5.10⁹ tons of sediment were transported into the Rhône delta system during this period, corresponding to an average of 3, 91.10⁶ tons/year (Fig. 9), with 7, 5.10⁹ tons of sand deposited in the early Rhône deltaic complex. According to Labaune et al. (2005), Berné et al. (2007), and Jouet et al. (2007), this volume seems to be underestimated, with the deposits possibly being 10% to 50% higher (Fig. 9).

5.1.2. From 7000 to 4300 Cal yr BP

This sequence corresponds to the first stage of progradation of the Rhône delta after the maximum flooding dated at 7000 Cal yr BP (Vella et al., 2005). This period records mainly the progradation of the St Ferréol and Ulmet lobes (Fig. 10). The estimated sediment flow was 5,4.10⁹ tons/year, a value greater than for the previous sequence (e.g., 11700-7000 Cal yr BP) (Fig. 9). Over this period, the rate of sea level rise decreased strongly (Fig. 10). However, this was compensated by the sediment flux arriving in the delta initiated by a transition from humid climate that prevailed during early Holocene to more arid conditions. This transition was also punctuated by frequent strong flooding episodes

affecting the watersheds of the northwestern Mediterranean region (Jalut et al., 2000; Benito et al., 2015; Jalali et al. 2017 ; Katrantsiosis et al., 2019). The increase in hydrosedimentary activity in the Rhône catchment area has also been reported, where, despite a period of hydrological quiescence in the basin, phases of increased hydrological activity occurred more often as observed by Berger et al., 2008; Arnaud et al., 2012 and Salvador and Berger, 2014. Two phases of fluvial-style metamorphosis from meandering to braided have been identified in the Upper Rhône (Salvador and Berger, 2014), the earliest around 7100 Cal yr BP and the second around 6100 Cal yr BP. These metamorphoses are linked with a large amount of sediment being released into the hydrological network.

The progradation was initiated thanks to two different distributary channels feeding the Saint-Ferréol and Ulmet lobes. The lack of data for the deltaic plain does not permit us to accurately estimate the distribution of deposits between the lobes, however, the sedimentary data analyzed in the study indicate that more than half of the flow passed through the Rhône of Saint-Ferréol (Fig. 5 and 10).

5.1.3. From 4300 to 3000 Cal yr BP

During this period, the sea level continued to rise slowly (1 m), and the sedimentary system records a second pulse of simultaneous progradation of both the St Ferreol and Ulmet lobes (Figs 5, 6 and 10). This second stage of progradation of these lobes was accentuated by an increase of the sediment flux compared to the previous cycle (i.e., 7000-4300 Cal yr BP), estimated $7,7 \cdot 10^9$ tons/year on average. There is no trace of a major distributary channel avulsion that could have diverted the course of the Rhône upstream of the delta.

During this period, two phases of increased activity in the hydrosystem are recorded in the Upper and Middle Rhône valley (Berger et al., 2007, 2008), the first between 4300 Cal yr BP to 3900 Cal yr BP, and the second between 3700 to 3500 Cal yr BP. Only the first phase is associated with a fluvial-braided river style in the Upper Rhône valley (Salvador and Berger, 2014) and a first maximum of Rhône fluvial detritism is recorded in the Bourget Lake (Arnaud et al., 2012). A coeval increase in agro-pastoral activity in the Northern Alps (Giguët-Covex et al., 2023) is also recorded during the Bronze Age (4150-

2700 Cal yr BP, Berger et al., 2019). These traces of human agro-pastoral activities in the Upper Rhône are also recorded in the Durance basin in the southeast of the catchment area at the same period (Miramont et al., 2004). The combined effect of punctuated strong floods periods together with the agro-pastoral activities that induced soil denudation and thus an increase of the erosion rate, could explain the drastic increase of sediment flux arriving in the delta at that period.

5.1.4. From 3000 to 2000 Cal yr BP

This period is characterized by a very important progradation phase of the Saint-Ferréol lobe (Figs. 5 and 10), and a slow-down of the Ulmet lobe progradation, which progressively dissociated from the Saint-Ferréol lobe. The sediment flux calculated over this period is of 21.10^9 tons/year. This value marks a big jump in terms of sediment flux compared to the previous sequence as it is three times greater (Fig. 9). This drastic increase of the sediment flux linked with a peak of the hydrological activity in the Rhône basin is due to the combination of several climatic and anthropic controlling factors.

Various climate events occurred during this period, which beginning is marked by a Bond event recorded in the northern hemisphere (Bond et al., 2001) that document large-scale multi centennial North-Atlantic cooling phases including West Mediterranean winter rain maxima (Zielhofer et al., 2019). A negative North Atlantic Oscillations (NAO) also prevailed during this period (Trouet et al., 2009; Faust et al., 2016) resulting in fewer and weaker winters with moist air brought in the Mediterranean (Hurrell et al., 2003). The consequences of these major climatic events resulted in an increase of the floods frequency at the scale of the Mediterranean (Benito et al., 2005) and in the Alps (Wirth et al., 2013). This is consistent with the torrential flow regime observed in the northern part of the Rhône basin (Salvador and Berger, 2014), with an increased hydrosedimentary activity at the Rhône/Saône confluence (Bravard et al., 1997). Evidences of significant flooding in the Durance basin are also reported at this period (Miramont et al., 2004). This higher precipitation regime is also supported by the observation of high lake levels in the Jura and the Northern Alps (both regions are located in the Northern Rhône basin) (Magny, 2004), with high rate of detrital transport and

sedimentation as observed in the Bourget lake in the northwestern Alps (Arnaud et al., 2013; Rapuc, 2022).

In addition, evidence of intense anthropisation is observed in the Middle Rhône Valley with many agricultural and pastoral indicators of a large regional vegetation impact (Berger et al., 2019), especially after 2200 cal BP during the late Gaulish and early Roman period, when the hydrosedimentary activity in the catchment area increased strongly, with intensive agropastoral practices (Bravard et al. 1997; Berger et al., 2008; Doyen et al., 2013).

5.1.5. From 2000 to 1000 Cal yr BP

This sequence corresponds to another key period for the Rhône delta development, with the onset of the Peccaïs lobe progradation to the east (Rey, 2006). There was therefore a major avulsion of anthropogenic origin (Rey et al., 2009), which was carried out to enable the hydrosedimentary flow to be re-oriented to the east of the delta.

The average sediment flow calculated for this period is $15,8 \cdot 10^9$ tons/year, which is moderately reduced compared to the 3000-2000 Cal yr BP period. The phase of intense hydrosedimentary activity initiated in the previous period continued (Berger et al., 2008), but is punctuated by periods of decreased hydrosedimentary activity of the Rhône basin with a braided fluvial style alternating with phases of meandering fluvial style. After 1500 Cal yr BP, the river system became braided again because of a strong hydrosedimentary load in the Upper Rhône valley (Salvador and Berger, 2014; Arnaud et al., 2012), and are not entirely correlated with the phase of activity in the Durance basin (Miramont et al., 2004).

Despite the decrease of the hydrosedimentary activity of the Rhône watershed, anthropogenic-associated herbaceous species progressively spread in place of trees in higher altitude settings after 1700 Cal yr BP (Brisset et al., 2015). This favored soil instability thus enhancing soil erosion and sediment release in the hydrosystem, which made the sediment volume observed in the system

substantial during this interval.

5.1.6. From 1000 Cal yr BP to the 18th century

This period had a strong impact on the Rhône delta evolution, with the Saint-Ferréol and Ulmet lobes becoming abandoned (Vella et al., 2005). The coastline in the axis of these abandoned lobes was then submitted to erosion. The Peccaïs lobe continued to prograde (Fig. 5), and a new lobe, the Bras De Fer lobe, started to develop in the south-east of the Ulmet lobe (Fig.s 5 and 6), due to anthropic-induced distributary channel avulsion of the St Ferréol/Ulmet towards the Bras de Fer.

This period records an important cooling in the North Atlantic region, corresponding to the Little Ice Age (LIA), started around 1300 E.C. and ending in 1850 CE (Mann et al., 2003).

The average sediment flow during this period was $25,5.10^9$ tons/year, which is higher than that for the previous period, and represents the highest average Rhône system sediment flow during the Holocene (Fig.s 9 and 109).

The intense hydrosedimentary activity that prevailed during this period coevals with an intense torrentiality of the Rhône River (Berger et al., 2008; Bravard, 2010). The Little Ice Age is also characterized by extreme anthropization of the catchment area with an important phase of deforestation and the development of arboriculture (including vineyards) (Berger et al., 2019). In addition to the anthropization of the catchment, the cold climatic conditions disrupted the watershed. Significant glacier development also occurred (Le Roy, 2012), which increased the sediment load in the rivers. Traces of significant torrentiality have been identified in several locations in the basin, including the Upper Rhône (Salvador and Berger, 2014), the confluence of the Saône river and the Rhône river in the city of Lyon (Landry et al., 2015), the Lower Rhône basin and Provence (Provansal and Morhange, 1994), and the Durance basin (Miramont et al., 2004), as well as a maximum of slackwater deposits in the Cevennes rivers (Dezileau et al., 2014). The combination of high anthropogenic pressure, low tree vegetation cover, and an extremely cold climate considerably altered the functioning of the catchment

and allowed a large amount of sediment to reach the delta.

5.1.7. From the 18th century to the present-day

During this last period, the Bras de Fer lobe became abandoned and the Roustan lobe started to develop, becoming the present-day main active lobe of the Rhône (Figs. 6 and 9).

The average flow is estimated at 14.10^9 tons/year (Fig. 9), that corresponds to almost the half than the sediment flow computed for the Little Ice Age period. If the resolution of the dating allowed it, this period could possibly be divided into two sub-periods. The older period before the 20th century would be characterized by strong sedimentary input echoing the second part of Little Ice Age, whereas the second period, after the middle of the 20th century, would be characterized by human superficialization of the Rhône River.

There are several reasons for the recent decrease in sediment supply. Since 1950, the construction of dams has severely reduced sediment transport by 80% (Bravard and Clemens, 2008; Provansal et al. 2014) compared to the last century. This reduction is due to sediment storage upstream of the dams and the subsequent reduced transport capacity of the original channel. The transport of gravel sized particles was reduced by a factor of 15 to 100 (Bravard and Clemens, 2008). In addition, a reforestation policy conducted in areas of medium and high altitude from the mid-19th century promoted soil preservation and reduced soil erosion and thus sediment load; a sedimentary deficit has been observed since the reduction of sedimentary inputs into the Rhône delta. Consequently, coastal erosion processes are not compensated by the sediment supply (Maillet et al., 2006a, b), and have reshaped the entire coastline except for the mouth of the Grand Rhône and the areas of convergence of the marine currents where the erosion products accumulate (Sabatier et al., 2006).

5.2. Dynamic of the Mediterranean deltas during the Holocene

Stratigraphic studies of the various Mediterranean deltas indicate a relatively similar development which can be summarized as a rapid marine transgression, a maximum flooding surface varying

between 7500 and 7000 Cal yr BP and then deltaic progradation at the scale of the Holocene (e.g., Bellotti et al., 1994; Sornoza et al., 1998; Vella et al., 2005; Arnaud-Fassetta and Suc, 2015; Amorosi et al. 2017; Pennington et al., 2017). The comparative study of the Ebro, the Pô, the Rhône deltas (Western Mediterranean) and the Nile delta (Eastern Mediterranean) was possible thanks to the availability of numerous published data on both watersheds and deltaic dynamic during the Holocene (Fig. 11). These four deltaic systems are amongst the most important in terms of watershed areas in the Mediterranean region resulting in a delta formation with substantial preservation, and their comparison was made possible due to the comparable climate conditions during the Holocene. Contrasted watershed systems however characterizes these four basins, that impacted differentially each of these delta dynamics.

In the western Mediterranean, the Holocene climate is characterized by a humid period that took place during the post Late Glacial Maximum progressive warming, punctuated by shorter arid periods (Benito et al., 2015; Fig. 11), until a transitional period towards a perennial aridification of the climate that initiated during the Mid-Holocene period. The following global aridification from the end of the Mid-Holocene onwards was also punctuated by short humid periods marked by more frequent floods periods (Magny et al., 1999; Benito et al., 2015). The West Mediterranean deltas (i.e., the Ebro, the Pô and the Rhône deltas) all record a same trend of transgressive coastal sedimentation during the period of humid and warming until a maximum sea invasion in the fluvial paleovalleys, corresponding to the Maximum Flooding Surface of the Holocene (around 7000 Cal yr BP), which is recorded at the onset of the climate transition towards aridification (Fig. 11). Above the Maximum Flooding Surface, these deltaic systems record an overall progradation until present, composed of higher frequency pulses of progradation which are not correlated in time (Fig. 11). These pulses correspond to the sedimentary response of the watershed local activity, linked with more local climate events that modulate the long-term trend that is recorded in the entire region. Indeed, each of these three systems have contrasted watersheds in terms of variability of sedimentary sources, relieves and types of climates. The Ebro River is sourced by the southern side of the Pyrenees, which correspond to a geographically

homogeneous high-altitude climate directly influenced by the North Atlantic climate. The Rhône system has a more contrasted watershed in terms of relief and climate belts, with subsequent contrasted hydrologic regimes (glacial and snow regimes in the eastern part (Alps), pluvial regime in the northern watershed (Saône basin), and the Cevennes regime in the western part of the mid-Rhône watershed (Dinh and Barthelemy, 2021). The Pô watershed is also contrasted, sourced in its Northern catchment in the Alps, and in its Southern catchment in the Apennines, as well submitted to contrasted hydrological regimes that result in the modulation of the global climate signal prevailing in western Mediterranean region (Benito et al., 2015). A destruction phase of these three deltas coupled with drastic decrease in sediment supply since the end of the Little Ice Age is recorded systematically with erosion of the coastal area and a progressive landward migration of the freshwater aquifer (Maseli and Trincardi, 2013).

The south-eastern Mediterranean region has also known a post Late Glacial Maximum warming phase characterized by the African Humid Period (AHP), followed by an arid period starting at the end of the Mid-Holocene until present-day, punctuated by short periods of extreme aridness periods (Zhao et al., 2020). The Nile delta is the biggest delta of the Mediterranean region, with the broadest watershed extending almost 4000km south of the Nile River mouth. During the Holocene, the Nile delta records a first transgressive phase linked with post Late Glacial Maximum rapid sea-level rise with coastal to estuarine deposits progressively covering the top Pleistocene surface (Stanley and Warne, 1998) up to the Maximum Flooding Surface highlighted by open marine prodelta sediments deposited on top of Early Holocene transgressive deposits (Coutellier and Stanley, 1987), dated around 7500 Cal yr BP at the onset of Mid-Holocene period (Marriner et al., 2012). This transgressive trend recorded in the Nile deltaic succession was followed by an overall deltaic progradation coeval to a stabilized slowdown of the sea-level rise and (Jouet, 2007). The Holocene Nile delta progradation is also punctuated by sedimentary pulses as evidences of short-term increase in sediment supply contemporary of short term periods of frequent strong flood events bounded by short extreme aridity periods recorded in the prodeltaic sediments (Zhao et al., 2020) (Fig. 11). The maximum progradation rate is reached

around 4000 Cal BP (Stanley and Warne, 1998), during the transition period between the African Humid Period (AHP) and the generalized aridification of the Nile basin. The Nile delta aggradation is then recorded with a generalized higher subsidence rate with a decrease in sediment supply (Pennington et al., 2017). The increasing anthropization of the Nile delta plain from 3000 Cal yr BP onwards also strongly control the rate of sediments arriving in the delta, since the Little Ice Age and particularly during the last century with the dam's construction (Stanley and Warne, 1998), with a drastic reduction of sediment supply resulting in fast rates of erosion of the delta.

5.3. Controlling factors on the relative sediment fluxes evolution

The temporal evolution of the sediment fluxes estimated for the Ebro, the Pô, the Nile and the Rhône delta during the Holocene are compared in the Fig. 11. The absolute values of sediment fluxes are not considered here as the volume of sediment is dependent on the size of the watersheds, and it is meaningless to compare absolute sediment fluxes values for Nile and Ebro, Pô and Rhône systems, the Nile watershed being at least three time bigger than any western Mediterranean watershed (Anthony et al., 2014). We therefore prefer to compare their evolutionary trends over the whole Holocene.

During the Early Holocene (e.g., 11700 to 7000 Cal yr BP), the four compared deltaic systems all record a major backstep while the relative sedimentary fluxes evaluated show different evolution patterns (low in the Rhône system, increasing in the Ebro system, decreasing in the Pô system, and highly fluctuating in the Nile system) (Fig. 11). The lower values in comparison with the post 7000 Cal yr BP periods may be due to generalized sediment starvation under conditions of rapid sea-level rise, that forced fluvial mouths to backstep, reducing sediment delivery to the coastal system. The hydrological stability that is recorded in the catchment area, punctuated by short events of greater hydrosedimentary activity (i.e., Bravard et al., 1997; Stanley and Warne, 1998; Corregiani et al., 2005; Frigola et al., 2007; Berger et al., 2008; Arnaud et al., 2012; Marriner et al., 2012; Berger, 2014 and Perez Lamban, 2018) is due to generally low vegetation density in the catchment area (Woodbridge et al., 2018). Despite the variability of sedimentary fluxes computed for different deltaic stings, the early

Holocene backstep is mainly controlled by the post-Pleistocene rapid sea-level rise, before the onset of the progradation, coeval to high sea-level stabilization.

During the mid- and late Holocene (after 7000 Cal yr BP), the overall progradation of the investigated deltas is not controlled either by a systematic increase of the sediment flux through time. Each of these deltas recorded several progradation pulses corresponding to different deltaic lobes growth phases linked with contrasted watershed activities. Both the Pô and the Ebro deltas show comparable flux evolution trends with two main phases of progressive increase from 7000 to around 4000 Cal yr BP and from 3500 Cal yr BP to the end of the Little Ice Age (Fig. 11), that seem to control the progradation pulses of both deltaic systems (Samoza et al., 1998; Amorosi et al., 2005). The Rhône and the Nile delta dynamics differ from that pattern. The Nile delta records a progressive decrease of sediment fluxes from 7000 Cal yr BP onwards (Marriner et al., 2012), whereas the delta shows a first period of progradation pulses around 6500 Cal yr BP and 3500 Cal yr BP, coeval to frequent flood periods recorded in the watershed (Zhao et al., 2020) (Fig. 11). It is followed by a period of aggradation of the delta plain linked with the combination of subsidence, decrease of sediment supply and intense anthropic activity impacting biosedimentary and hydrological budget through irrigation and culture development (Pennington et al. 2017).

Concerning the Rhône delta, a first interval until around 3000 Cal yr BP is characterized by the onset of the progradation of both Ulmet and St-Ferreol lobes, with a progressive increase of the sediment flux coeval to the stabilization of the sea-level. The sediment fluxes drastically increase after 3000 Cal yr BP with two important pulses, a first dated from the end of the Iron Age to the early Roman period (Fig. 11) with increasing anthropic pressure on the watershed and on the delta plain, and a second corresponding to the Little Ice Age with anthropic denudation of the watershed vegetation cover inducing higher erosion, connectivity and sediment transport to the delta.

The near-opposition of the hydrosedimentary flow curves of the Rhône and Nile rivers clearly illustrates the opposing climatic gradients on either side of the Mediterranean basin during the

Holocene, and the inversions that were to mark their respective watersheds at the hinge in time corresponding to the end of the African Humid period around 6000/5500 Cal yr BP. The southern Mediterranean basin was then wetter than the north, then dried out as the northern European basins became wetter and cooler (especially from the 45th parallel north onwards, with strengthening Westerlies and glacial descents (Magny et al., 2013). The primary forcing factor here does indeed seem to be climatic under orbital forcing, with a stronger anthropogenic amplification in the Rhône basin from 3000 Cal yr BP onwards. The orbital forcing evolution curve from Berger and Loutre (1991) in Fig. 11 shows the intersection of the curves of highest summer and winter insolation corresponding to the intersection of the anticorrelated hydrosedimentary flux curves of the two major basins.

6. Conclusion

The calculation of the sediments volumes associated with the different phases of construction of the deltaic system of the Rhône over the last 11 700 years highlights the relationship between the catchment area and the delta. The results were obtained thanks to the high-resolution stratigraphic study of sediment cores (including 25 new radiocarbon dates for the delta in addition to the ones available in the literature. High resolution stratigraphic correlations completing existing seismic interpretation of the Rhône delta made it possible to produce the topographic map for 12 500 Cal yr BP corresponding to the initial surface on which the Rhône delta developed and helped at estimating the volume of sediment deposited in the system. The early Rhône deltaic complex, a protodelta, initially developed because of a slowdown in the rise in sea level (during the Late Dryas period), and it took almost 3000 years for the Rhône delta to start its development. Changes in sedimentary volumes around 7000 Cal yr BP reflect the turnaround from a backstepping coastal system punctuated by short-lived phases of progradation (early Rhône deltaic complex) to a markedly prograding system. Middle to late Holocene estimated sedimentary volumes could be associated with different development phases and related to hydroclimatic events in the catchment area. Sedimentation rate changes related

to periods of climatic and anthropogenic forcings are identified: The period centered around 3000 Cal yr BP seems to represent a major bifurcation in the history of the Rhône delta and its watershed, with human forcing becoming more widespread and intensive from this period onwards. The sedimentary data required to study sediment budgets evolution in deltaic systems are available for many Holocene deltas, and comparative studies of sediment volumes is made possible.

A comparative synthesis of the main Mediterranean deltaic systems (the Nile, the Pô, the Rhône and the Ebro) show that the deltaic architectures have similar stratigraphic trends with a phase of retrogradation from 11700 Cal yr BP to 7000 Cal yr BP followed by a generalized deltaic progradation, which shorter term pulses are controlled by local climates prevailing in contrasted watersheds, and by the progressive anthropization of the different basins from 3000 Cal yr BP onwards. The Holocene sediment fluxes trends from eastern and western Mediterranean are anticorrelating and controlled by opposite climatic gradients on either side of the Mediterranean basin.

Acknowledgements

This work has been supported by IFP Energies nouvelles in the frame of internal funded research project, in collaboration with Lyon 2 University, IFREMER, CEREGE and Bologna University. We also acknowledge the two anonymous reviewers and the editors that helped at greatly improve the manuscript. The authors of this manuscript declare that there is no conflict of interest.

Data availability

The data used in this study can be made available to readers if a request is made to the corresponding author.

References

Allen, J. R., 1963. The classification of cross-stratified units. With notes on their

origin. *Sedimentology*, 2(2), 93-114.

Allen, J. R., 1965. A review of the origin and characteristics of recent alluvial sediments. *Sedimentology*, 5(2), 89-191.

Amorosi, A. and Milli, S., 2001. Late Quaternary depositional architecture of Po and Tevere river deltas (Italy) and worldwide comparison with coeval deltaic successions. *Sedimentary geology*, 144(3-4), 357-375.

Amorosi, A., Centineo, M. C., Colalongo, M. L., Fiorini, F., 2005. Millennial-scale depositional cycles from the Holocene of the Po Plain, Italy. *Marine Geology*, 222, 7-18.

Amorosi, A., Rossi, V., Vella, C., 2013. Stepwise post-glacial transgression in the Rhône Delta area as revealed by high-resolution core data. *Palaeogeography, Palaeoclimatology, Palaeoecology*, 374, 314-326.

Amorosi, A., Bruno, L., Campo, B., Costagli, B., Pinelli, E., Hong, W., Sammartino, I., Vaiani, S.C., 2020. Tracing clinothem geometry and sediment pathways in the prograding Holocene Po Delta system through integrated core stratigraphy. *Basin Research* 32 (1-10), 206e215. <https://doi.org/10.1111/bre.12360>

Anthony, E.J., Marriner, N., Morhange, C., 2014. Human influence and the changing geomorphology of Mediterranean deltas and coasts over the last 6000 years: From progradation to destruction phase? *Earth-Science Reviews* 139 (2014) 336–361.

Archaeomedes, E., 1998. Des oppida aux métropoles. *Anthropos, collection Villes, Paris*) 290p.

Arnaud, F., Révillon, S., Debret, M., Revel, M., Chapron, E., Jacob, J., Giguët-Covex, C., Poulénard, J., Magny, M., 2012. Lake Bourget regional erosion patterns reconstruction reveals Holocene NW European Alps soil evolution and paleohydrology. *Quaternary Science Reviews*, 51, 81-92.

Arnaud-Fassetta, G., 1999. Dynamiques fluviales holocènes dans le delta du Rhône. *L'Information géographique*, 63(1), 37-38.

Arnaud-Fassetta, G., 2002. Geomorphological records of a 'flood-dominated regime' in the Rhône Delta (France) between the 1st century BC and the 2nd century AD. What correlations with the catchment paleohydrology? *Geodinamica Acta*, 15(1), 79-92.

Arnaud-Fassetta, G., Provansal, M., 1993. Étude géomorphologique du delta du Rhône: évolution des milieux de sédimentation fluviales au cours de l'Holocène récent. *Méditerranée: revue géographique des pays méditerranéens*, 78(3-4), 31-42.

Arnaud-Fassetta, G., & Provansal, M., 1999. High frequency variations of water flux and sediment discharge during the Little Ice Age (1586–1725 AD) in the Rhône Delta (Mediterranean France). Relationship to the catchment basin. *Man and River Systems: The Functioning of River Systems at the Basin Scale*, 241-250.

Arnaud-Fassetta, G., Suc, J. P., 2015. Dynamique hydrogéomorphologique et diversité végétale dans le delta du Rhône (France) de -10 000 ans à demain. *Cahiers de Vallesia*, 29, Sion, 2015, p. 63-98.

Bard, E., Hamelin, B., Delanghe-Cabatièr, D., 2010. Deglacial meltwater pulse 1B and Younger Dryas sea levels revisited with boreholes at Tahiti. *Science*, 327(5970), 1235-1237.

Bassetti, M. A., Jouet, G., Dufois, F., Berné, S., Rabineau, M., Taviani, M., 2006. Sand bodies at the shelf edge in the Gulf of Lions (Western Mediterranean): Deglacial history and modern processes. *Marine Geology*, 234(1-4), 93-109.

Beeching, A., Brochier, J. L., Cordier, F., 2000. La transition Mésolithique-Néolithique entre la plaine du Rhône moyen et ses bordures préalpines. *Les Paléoalpins, Hommage a Pierre Bintz, Géologie Alpine, Mémoire Hs*, 31, 201, 210.

Bellotti, P., Chiocci, F. L., Milli, S., Tortora, P., Valeri, P., 1994. Sequence stratigraphy and depositional

setting of the Tiber Delta; integration of high-resolution seismics, well logs, and archeological data. *Journal of Sedimentary Research*, 64(3b), 416-432.

Benito, G., Macklin, M.G., Zielhofer, C., Jones, A.F., Machado, M.J., 2015. Holocene flooding and climate change in the Mediterranean. *CATENA*, Volume 130, Pages 13-33.

Berger, A. L., 1977. Support for the astronomical theory of climatic change. *Nature*, 269, 44-45.

Berger, A., 1978. Long-term variations of daily insolation and Quaternary climatic changes. *Journal of Atmospheric Sciences*, 35(12), 2362-2367.

Berger, J. F., 2003. La «dégradation des sols» à l'Holocène dans la moyenne vallée du Rhône: contextes morpho-climatique, paléobotanique et culturel, chapitre 3. Les facteurs de l'érosion: modes d'analyse et conceptualisation des processus, chapitre 4: Les étapes de la morphogenèse holocène dans le sud de la France. Archéologie et systèmes socio-environnementaux. Etudes multiscalaires sur la vallée du Rhône dans le programme Archaeomedes. Paris, CNRS, 2003, 43-161.

Berger, A., Loutre, M. F., 1991. Insolation values for the climate of the last 10 million years. *Quaternary Science Reviews*, 10(4), 297-317.

Berger, J.F., Brochier, J.L., Vital, J., Delhon, C., Thiébaud, S., 2007. Nouveau regard sur la dynamique des paysages et l'occupation humaine à l'Âge du Bronze en moyenne vallée du Rhône. Environnements et cultures à l'Âge du Bronze en Europe occidentale, Paris, Éd. du CTHS (Documents préhistoriques), 21, 259-284.

Berger, J.F., Salvador, P.G., Franc, O., Verot-Bourrely, A., Bravard, J.P., 2008. La chronologie fluviale postglaciaire du haut bassin rhodanien. Collection EDYTEM. *Cahiers de géographie*, 6(1), 117-144.

Berger, J.F., Delhon, C., Magnin, F., Bonte, S., Peyric, D., Thiebault, S., Beeching, A., 2016. A fluvial record of the mid-Holocene rapid climatic changes in the middle Rhône valley (Espeluche-Lalo, France) and of their impact on Late Mesolithic and Early Neolithic societies. *Quaternary Science Reviews*, 136,

66-84.

Berger, J.F., Shennan, S., Woodbridge, J., Palmisano, A., Mazier, F., Nuninger, L., Roberts, C.N., 2019. Holocene land cover and population dynamics in Southern France. *The Holocene*, 29(5), 776-798.

Berné, S., Jouet, G., Bassetti, M.A., Dennielou, B., Taviani, M., 2007. Late Glacial to Preboreal sea-level rise recorded by the Rhône deltaic system (NW Mediterranean). *Marine Geology*, 245(1-4), 65-88.

Bernhardt, C.E., Stanley, J.-D., Horton, B.P., 2011. Wetland vegetation in Manzala lagoon, Nile delta coast, Egypt: Rapid responses of pollen to altered Nile hydrology and land use. *Journal of Coastal Research*, v. 274, p. 731–737, doi:10.2112/10A-00001.1.

Bernhardt, C.E., Horton, B.P., Stanley, J.D., 2012. Nile Delta vegetation response to Holocene climate variability. *Geology*, 40(7), 615-618.

Bhattacharya, J.P., Giosan, L., 2003. Wave-influenced deltas: Geomorphological implications for facies reconstruction. *Sedimentology*, 50(1), 187-210.

Bladé, I., Liebmann, B., Fortuny, D., Van Oldenborgh, G.J., 2012. Observed and simulated impacts of the summer NAO in Europe: implications for projected drying in the Mediterranean region. *Climate dynamics*, 39, 709-727.

Bond, G.C., Lotti, R., 1995. Iceberg discharges into the North Atlantic on millennial time scales during the last glaciation. *Science*, 267(5200), 1005-1010.

Boudet, L., Sabatier, F., Radakovitch, O., 2017. Modelling of sediment transport pattern in the mouth of the Rhône delta: Role of storm and flood events. *Estuarine, Coastal and Shelf Science*, 198, 568-582.

Bravard, J.P., 1997. Géoarchéologie des vallées alluviales de Rhône-Alpes depuis le Tardiglaciaire. *Documents d'Archéologie Rhône-Alpes*, 129-150.

Bravard, J. P., 2010. Discontinuities in braided patterns: The River Rhône from Geneva to the Camargue

delta before river training. *Geomorphology*, 117(3-4), 219-233.

Bravard, J. P., Clémens, A., 2008. Le Rhône en 100 questions (p. 295). ZABR, Zone Atelier Bassin du Rhône.

Bravard, J.P., Landon, N., Peiry, J.L., Piégay, H, 1999. Principles of engineering geomorphology for managing channel erosion and bedload transport, examples from French rivers. *Geomorphology*, 31(1-4), 291-311.

Brisset, E., Guiter, F., Miramont, C., Revel, M., Anthony, E. J., Delhon, C., De Beaulieu, J.L., 2015. Late glacial/Holocene environmental changes in the Mediterranean Alps inferred from lacustrine sediments. *Quaternary Science Reviews*, 110, 49-71.

Chiocci, F.L., Ercilla, G., Torre, J., 1997. Stratal architecture of Western Mediterranean Margins as the result of the stacking of Quaternary lowstand deposits below 'glacio-eustatic fluctuation base-level'. *Sedimentary Geology*, 112(3-4), 195-217.

Clauzon, G., Suc, J. P., Gautier, F., Berger, A., Loutre, M.F., 1996. Alternate interpretation of the Messinian salinity crisis: controversy resolved? *Geology*, 24(4), 363-366.

Coleman, J. M., Roberts, H.H., Stone, G. W., 1998. Mississippi River delta: an overview. *Journal of Coastal Research*, 699-716.

Colomb, E., Gieu, G., Masse, J. P., Rouire, J., Roux, M., 1975. Notice de la Carte Géologique 1/50 000, Feuille 1018 d" Istres.

Goineau, A., Fontanier, C., Jorissen, F.J., Lansard, B., Buscail, R., Mouret, A., Kerhervé, P., Zaragosi, S., Ernoult, E., Artéro, C., Anschutz, P., Metzger, E., Rabouille, C., 2011. Live (stained) benthic foraminifera from the Rhône prodelta (Gulf of Lion, NW Mediterranean): Environmental controls on a river-dominated shelf. *Journal of Sea Research*, 65(1), 58-75.

Correggiani, A., Cattaneo, A., Trincardi, F., 2005. The modern Po Delta system: lobe switching and

asymmetric prodelta growth. *Marine Geology* 222–223, 49–74.

Coutellier, V. Stanley, D.J., 1987. Late Quaternary stratigraphy and paleogeography of the eastern Nile Delta, Egypt. *Marine Geology* 77: 257-275.

Debret, M., Chapron, E., Desmet, M., Rolland-Revel, M., Magand, O., Trentesaux, A., Arnaud, F., 2010. Northwestern Alps Holocene paleohydrology recorded by flooding activity in Lake Le Bourget, France. *Quaternary science reviews*, 29(17-18), 2185-2200.

Denton, G.H., Karlén, W., 1973. Holocene climatic variations—their pattern and possible cause. *Quaternary Research*, 3(2), 155-205.

Dezileau, L., Terrier, B., Berger, J. F., Blanchemanche, P., Jacopin, A., Freydier, R., Delgado, J. L., 2014. Reconstitution des crues extrêmes du Gardon à partir d'une analyse paléohydrologique. *La Houille Blanche*, (4), 44-52.

Dietrich, W. E., Kirchner, J. W., Ikeda, H., Iseya, T., 1989. Sediment supply and the development of the coarse surface layer in gravel-bedded rivers. *Nature*, 340(6230), 215-217.

Dinh, T.V., Barthelemy, L., 2021. Climate variability and extreme weather events in the Mediterranean region. Université Grenoble Alpes technical report. DOI: 10.13140/RG.2.2.29330.38080.

Dott Jr, R.H., Bourgeois, J., 1982. Hummocky stratification: significance of its variable bedding sequences. *Geological Society of America Bulletin*, 93(8), 663-680.

Doyen, É., Vannièrè, B., Berger, J.F., Arnaud, F., Tachikawa, K., Bard, E., 2013. Land-use changes and environmental dynamics in the upper Rhone valley since Neolithic times inferred from sediments in Lac Moras. *The Holocene*, 23(7), 961-973.

Dung, B. V., 2013. Late Pleistocene–Holocene seismic stratigraphy of the Southeast Vietnam shelf. Lion (Doctoral dissertation, Kiel).

Elliott, T., 1976. Upper Carboniferous sedimentary cycles produced by river-dominated, elongate deltas. *Journal of the Geological Society*, 132(2), 199-208.

Elliott, T., 1986. Deltas, in Reading, H.G., ed., *Sedimentary Environments and Facies*: Oxford, U.K., Blackwell Scientific Publications, p. 113–154.

Embry, A.F., 2002. Tectonic and eustatic signals in the sequence stratigraphy of the Upper Devonian Canadaway Group, New York state: Discussion. *AAPG bulletin*, 86(4), 695-695.

Embry, A., 2009. Crockerland—The Source Area for the Triassic to Middle Jurassic Strata of Northern Axel Heiberg Island, Canadian Arctic Islands. *Bulletin of Canadian Petroleum Geology*, 57(2), 129-140.

Fanget, A.S., Bassetti, M.A., Arnaud, M., Chiffolleau, J.F., Cossa, D., Goineau, A., Berné, S., 2013. Historical evolution and extreme climate events during the last 400 years on the Rhône prodelta (NW Mediterranean). *Marine Geology*, 346, 375-391.

Fanget, A.S., Berné, S., Jouet, G., Bassetti, M.A., Dennielou, B., Maillet, G.M., Tondut, M., 2014. Impact of relative sea level and rapid climate changes on the architecture and lithofacies of the Holocene Rhône subaqueous delta (Western Mediterranean Sea). *Sedimentary Geology*, 305, 35-53.

Foix, N., Paredes, J.M., Giacosa, R.E., 2013. Fluvial architecture variations linked to changes in accommodation space: Río Chico Formation (late Paleocene), Golfo San Jorge basin, Argentina. *Sedimentary Geology*, 294, 342-355.

Frigola, J., Moreno, A., Cacho, I., Canals, M., Sierro, F. J., Flores, J. A., Grimalt, J. O., Hodell, D. A., and Curtis, J. H., 2007, Holocene climate variability in the western Mediterranean region from a deepwater sediment record. *Paleoceanography*, 22, PA2209, doi:10.1029/2006PA001307.

Gasse, F., 2000. Hydrological changes in the African tropics since the Last Glacial Maximum. *Quaternary Science Reviews*, 19(1-5), 189-211.

Gensous, B., Tesson, M., 2003. L'analyse des dépôts postglaciaires et son application à l'étude des

séquences de dépôt du Quaternaire terminal sur la plate-forme au large du Rhône (golfe du Lion). *Bulletin de la Société Géologique de France*, 174(4), 401-419.

Gertsch, B., Keller, G., Adatte, T., Berner, Z., Kassab, A.S., Tantawy, A.A.A., Stueben, D., 2010. Cenomanian–Turonian transition in a shallow water sequence of the Sinai, Egypt. *International Journal of Earth Sciences*, 99, 165-182.

Giguet-Covex, C., Bajard, M., Chen, W., Walsh, K.J., Rey, P.J., Messenger, E., Poulencard, J., 2023. Long-term trajectories of mountain agro-ecosystems in the North-Western Alps. *Regional Environmental Change*, 23(2), 58.

Goiran, J.P., Morhange, C., Bourcier, M., Carbonel, P., and Morigi, C., 2000. Évolution des rivages d'Alexandrie à l'Holocène récent, marge occidentale du delta du Nil, Egypte. *Méditerranée*, 94(1), 83-90.

Got, H, Aloisi, J.C., Monaco, A., 1985. Sedimentary processes in Mediterranean deltas and shelves. D. J. Stanley et al. (eds.), *Geological Evolution of the Mediterranean Basin*, © Springer-Verlag New York, Inc. 1985

Got, H., Aloisi, J.C., 1990. The Holocene sedimentation on the Gulf of Lions margin: a quantitative approach. *Continental Shelf Research*, 10(9-11), 841-855.

Grioulet, C., 1976. Hydrodynamique et hydrochimie du complexe aquifère de haute et moyenne Camargue, Acte de colloque : Hydrogeology of great sedimentary Bassins. IAH-IAHS, Budapest, Hongrie, 351-369.

Grove, J.M., 1988: The Little Ice Age. London: Routledge, xxii + 498 pp. *Progress in Physical Geography: Earth and Environment*, 32(1), 103–106.

Guilaine, J., Manen, C., 2005. From Mesolithic to early Neolithic in the western Mediterranean. In *Going over: The Mesolithic-Neolithic Transition in the North-West Europe* (pp. 21-51). Oxford

University Press.

Guimerá, J., Mariano, A., 1990. Structure et évolution de la compression alpine dans la Chaîne Ibérique et la Chaîne côtière catalane (Espagne). *Bulletin de la Société géologique de France*, 6(2), 339-348.

Gustavs, I., 1992. Rechnergestützte Inversion und Modellierung des Kompaktionsprozesses von Sedimenten. Diploma thesis, Ernst Moritz Arndt University, Greifswald.

Heaton, T.J., Köhler, P., Butzin, M., Bard, E., Reimer, R.W., Austin, W.E., Ramsey, C.B., Grootes, P.M., Hughen, K.A., Kromer, B., Reimer, P.J., Adkins, J., Burke, A., Cook, A.B., Olsen, J., Skinner, L.C., 2020. Marine20—The Marine Radiocarbon Age Calibration Curve (0–55,000 cal BP). *Radiocarbon*. 2020;62(4):779-820. doi:10.1017/RDC.2020.68

Hijma, M.P., and Cohen, K.M., 2011. Holocene transgression of the Rhine River mouth area, The Netherlands/Southern North Sea: palaeogeography and sequence stratigraphy. *Sedimentology*, 58(6), 1453-1485.

Holzhauser, H., Magny, M., Zumbühl, F., 2005. Glacier and lake-level variations in west-central Europe over the last 3500 years. *The Holocene*, 15(6), 789-801.

Hurrell, J.W., Kushnir, Y., Cotterton, G., Visbeck, M., 2003. An overview of the North Atlantic Oscillation. *Geophysical Monograph*, American Geophysical Union 2003, 134, 1–36.

Jalali, B., Sicre, M.A., Bassetti, M.A., & Kallel, N., 2017. Holocene climate variability in the north-western Mediterranean Sea (gulf of lions). *Climate of the Past*, 12(1), 91-101

Jalut, G., Amat, A.E., Bonnet, B., Gauquelin, T., Fontugne, M., 2000. Holocene climatic changes in the Western Mediterranean, from south-east France to south-east Spain. *Palaeogeography, Palaeoclimatology, Palaeoecology*, Volume 160, Issues 3–4, pp 255-290.

Jauzein, A., 1971. Les agents de la morphogénèse – Les eaux courantes. *Trav. Lab. Géol. ENS.*, 5, 177p.

- Jouët, G., 2007. Enregistrements stratigraphiques des cycles climatiques et glacio-eustatiques du Quaternaire terminal: modélisations de la marge continentale du Golfe du Lion (Doctoral dissertation, Brest).
- Labaune, C., Jouet, G., Berné, S., Gensous, B., Tesson, M., Delpeint, A., 2005. Seismic stratigraphy of the Deglacial deposits of the Rhône prodelta and of the adjacent shelf. *Marine Geology*, 222, 299-311.
- Lambeck, K., Esat, T.M., Potter, E.K., 2002. Links between climate and sea levels for the past three million years. *Nature*, 419(6903), 199-206.
- Landry, C., Pasty, J.F., Alix, P., Brouillaud, S., Franc, O., Vermeulen, C., 2015. Nouveaux indices de fréquentation de la vallée inférieure de la Saône au Paléolithique moyen et supérieur. *Bulletin de la Société préhistorique française*, 112(4), 791-795.
- Lefebvre, D., 1980. Evolution morphologique et structurale du golfe du Lion, essai de traitement statistique des données. These, Univ. Paris, Paris, 163 pp.
- Le Roy, M., Nicolussi, K., Deline, P., Astrad, J., Edouard, J.L., Miramont, C., Arnaud, F., 2015. Calendar-dated glacier variations in the western European Alps during the Neoglacial: the Mer de Glace record, Mont Blanc massif. *Quaternary Science Reviews*, 108, 1-22.
- Liébault, F., Piégay, H., 2002. Causes of 20th century channel narrowing in mountain and piedmont rivers of southeastern France. *Earth Surface Processes and Landforms: The Journal of the British Geomorphological Research Group*, 27(4), 425-444.
- Luterbacher H.P., 1970. Environmental distribution of early Tertiary microfossils, Tremp Basin, Northeastern Spain. ESSo Production Research, EPR-E-1ER-70, Bègles, 1-48.
- Magny, M., 2004. Fluctuations du niveau des lacs dans le Jura, les Préalpes françaises du Nord et le Plateau suisse, et variabilité du climat pendant l'Holocène. *Méditerranée*, 102(1), 61-70.
- Magny, M., Arnaud, F., Holzhauser, H., Chapron, E., Debret, M., Desmet, M., Vannière, B., 2010. Solar

and proxy-sensitivity imprints on paleohydrological records for the last millennium in west-central Europe. *Quaternary Research*, 73(2), 173-179.

Magny, M., Joannin, S., Galop, D., Vanni re, B., Haas, J.N., Bassetti, M., Desmet, M., 2012. Holocene palaeohydrological changes in the northern Mediterranean borderlands as reflected by the lake-level record of Lake Ledro, northeastern Italy. *Quaternary Research*, 77(3), 382-396.

Magny, M., Combourieu-Nebout, N., De Beaulieu, J.L., Bout-Roumazielles, V., Colombaroli, D., Desprat, S., Wirth, S., 2013. North–south palaeohydrological contrasts in the central Mediterranean during the Holocene: tentative synthesis and working hypotheses. *Climate of the Past*, 9(5), 2043-2071.

Maillet, G., 2005. Relations s dimentaires r centes et actuelles entre un fleuve et son delta en milieu microtidal: exemple de l'embouchure du Rh ne (Doctoral dissertation, Universit  de Provence-Aix-Marseille I).

Maillet, G.M., Sabatier, F., Rousseau, D., Provansal, M., and Fleury, T.J., 2006a. Connexions entre le Rh ne et son delta (partie 1):  volution du trait de c te du delta du Rh ne depuis le milieu du XIXe si cle. *G omorphologie: relief, processus, environnement*, 12(2), 111-124.

Maillet, G.M., Vella, C., Provansal, M., Sabatier, F., 2006b. Connexions entre le Rh ne et son delta (partie 2):  volution du trait de c te du delta du Rh ne depuis le d but du XVIIIe si cle. *G omorphologie: relief, processus, environnement*, 12(2), 125-140.

Mann, M.E., Bradley, R.S., Hughes, M.K., 1999. Northern Hemisphere Temperatures during the Past Millennium: Inferences, Uncertainties, and Limitations, *Geophysical Research Letters*, 26, 759–762.

Mann, M.E., Zang, Z., Rutherford, S. Bradley, R.S., Hughes, M.K., Shindell, D., Ammann, C., Faluvegi, G., Fenbiao, N., 2009. Global Signatures and Dynamical Origins of the Little Ice Age and Medieval Climate Anomaly. *Science*, vol. 326, 2009, pp. 1256 – 1260.

Marriner, N., Flaux, C., Morhange, C., Kaniewski, D., 2012. Nile Delta's sinking past: Quantifiable links

with Holocene compaction and climate-driven changes in sediment supply? *Geology* 40 (12), 1083–1086.

Maselli, V., Trincardi, F., 2013. Man made deltas. *Scientific Reports* 3, 1926 (2013). doi.org/10.1038/srep01926

Mateu-Vicens, G., Brandano, M., Gaglianone, G., and Baldassarre, A., 2012. Seagrass-meadow sedimentary facies in a mixed siliciclastic–carbonate temperate system in the Tyrrhenian Sea (Pontinian Islands, Western Mediterranean). *Journal of Sedimentary Research*, 82(7), 451-463.

McPherson, J. G., Shanmugam, G., Moiola, R. J., 1987. Fan-deltas and braid deltas: varieties of coarse-grained deltas. *Geological Society of America Bulletin*, 99(3), 331-340.

Miall, A. D., 2014. Fluvial depositional systems (Vol. 14, p. 316). Cham: Springer International Publishing.

Milankovitch, M.M., 1941. Canon of insolation and the iceage problem. Koniglich Serbische Akademie *Beograd Special Publication*, 132.

Miramont, C., Rosique, T., Sivan, C., Edouard, J.L., Magnin, F., Talon, B., 2004. Le cycle de sédimentation «postglaciaire principal» des bassins marneux subalpins: état des lieux. *Méditerranée*, 102(1), 71–84.

Morgan, R.P.C., 2009. Soil Erosion and Conservation. John Wiley & Sons, Hoboken.

Mutti, E., Tinterri, R., Di Biase, D., Fava, L., Mavilla, N., Angella, S., Calabrese, L., 2000. Delta-front facies associations of ancient flood-dominated fluvio-deltaic systems. *Revista de la Sociedad Geológica de España*, 13(2), 165-190.

Nelson, J. M., Smith, J. D., 1989. Evolution and stability of erodible channel beds. *River meandering*, 12, 321-377.

- Nicholls, R.J., Adger, W.N., Hutton, C.W., Hanson, S.E., 2020. Deltas in the Anthropocene (p. 282). *Springer Nature*.
- Notebaert, B., Berger, J.F., 2014. Quantifying the anthropogenic forcing on soil erosion during the Iron Age and Roman Period in southeastern France. *Anthropocene*, 8, 59-69.
- Olivero, E. B., Malumián, N., 2008. Mesozoic-cenozoic stratigraphy of the fuegian Andes, Argentina. *Geologica Acta: an international earth science journal*, 6(1), 5-18.
- Oomkens, E., 1970. Depositional sequences and sand distribution in the postglacial Rhône delta complex. *Deltaic Sedimentation, Modern and Ancient*, James P. Morgan, Robert H. Shaver.
- Orton, G.J., Reading, H.G., 1993. Variability of deltaic processes in terms of sediment supply, with particular emphasis on grain size. *Sedimentology*, 40(3), 475-512.
- Palanques, A., de Madron, X.D., Puig, P., Fabres, I., Quillén, J., Calafat, A., Bonnin, J., 2006. Suspended sediment fluxes and transport processes in the Gulf of Lions submarine canyons. The role of storms and dense water cascading. *Marine Geology*, 234(1-4), 43-61.
- Pemberton, S.G., 1992. Applications of ichnology to petroleum exploration (Vol. 17, pp. 141-167). *SEPM Society for Sedimentary Geology*.
- Pennington, B.T., Sturt, F., Wilson, P., Rowland, J., Brown, A.G., 2017. The fluvial evolution of the Holocene Nile Delta. *Quaternary Science Reviews*, 170, 212-231.
- Pérez-Lambán, F., Peña-Monné, J.L., Badía-Villas, D., Picazo Millán, J.V., Sampietro-Vattuone, M.M., Alcolea Gracia, M., Aranbarri, J., González-Sampériz, P., Fanlo Loras, J., 2018. Holocene environmental variability in the Central Ebro Basin (NE Spain) from geoarchaeological and pedological records. *Catena* 163.
- Petts, G.E., Gurnell, A.M., 2005. Dams and geomorphology: research progress and future directions. *Geomorphology*, 71(1-2), 27-47.

Pichard, G., 2017. Alain Coulomb, Le marégraphe de Marseille. De la détermination de l'origine des altitudes au suivi des changements climatiques. 130 ans d'observations du niveau de la mer. 2014, Presses des Ponts, 633 p., ISBN: 978-2-85978-481-2. Méditerranée. *Revue géographique des pays méditerranéens/Journal of Mediterranean geography*, (128), 69.

Pichard, G., Roucaute, E., 2014. Sept siècles d'histoire hydroclimatique du Rhône d'Orange à la mer (1300–2000), climat, crues, inondations. *Méditerranée*, 122, 31-42.

Provansal, M., 2005. Relations sédimentaires récentes et actuelles entre un fleuve et son delta en milieu microtidal: Exemple de l'embouchure du Rhône (Doctoral dissertation, Université Aix-Marseille).

Provansal, M., Morhange, C., 1994. Seuils climatiques et réponses morphogéniques en Basse-Provence depuis 5000 ans [Climatic threshold and morphogenesis in Basse-Provence since 5000 years]. *Quaternaire*, 5(3-4), 113-118.

Provansal, M., Vella, C., Arnaud-Fassetta, C., Sabatier, F., Maillet, G., 2003. Role of fluvial sediment inputs in the mobility of the Rhône delta coast (France)/Participation des apports sédimentaires fluviaux à la mobilité du littoral du delta du Rhône (France). *Géomorphologie: relief, processus, environnement*, 9(4), 271-287.

Provansal, M., Dufour, S., Sabatier, F., Anthony, E.J., Raccasi, G., Robresco, S., 2014. The geomorphic evolution and sediment balance of the lower Rhône River (southern France) over the last 130 years: Hydropower dams versus other control factors. *Geomorphology*, 219, 27-41.

Rabineau, M., Berné, S., Aslanian, D., Olivet, J. L., Joseph, P., Guillocheau, F., Granjeon, D., 2005. Sedimentary sequences in the Gulf of Lion: a record of 100,000 years climatic cycles. *Marine and Petroleum Geology*, 22(6-7), 775-804.

Reimer, P.J., Austin, W. E., Bard, E., Bayliss, A., Blackwell, P.G., Ramsey, C.B., Talamo, S., 2020. The

IntCal20 Northern Hemisphere radiocarbon age calibration curve (0–55 cal kBP). *Radiocarbon*, 62(4), 725-757.

Renaud, F.G., Kuenzer, C., 2012. The Mekong Delta System: Interdisciplinary 7 Analyses of a River Delta. *Springer Environmental Science and Engineering*, DOI 10.1007/978-94-007-3962-8_2, © Springer Science+Business Media Dordrecht 2012

Rey, T., 2006. Dynamiques hydro-sédimentaires en Petite Camargue à l'Holocène (Doctoral dissertation, Université Paul Valéry-Montpellier III).

Rey, T., Lefevre, D., Vella, C., 2009. Deltaic plain development and environmental changes in the Petite Camargue, Rhône Delta, France, in the past 2000 years. *Quaternary Research*, 71(3), 284-294.

Rossiaud, J., 1994. Réalités et imaginaire d'un fleuve: recherches sur le Rhône médiéval (Doctoral dissertation, Paris 1).

Sabatier, F., 2001. Fonctionnement et dynamiques morpho-sédimentaires du littoral du delta du Rhône (Doctoral dissertation, Aix-Marseille 3).

Sabatier, F., Maillet, G., Provansal M., Fleury, T. J., Suanez, S., Vella, C., 2006. Sediment budget of the Rhône delta shoreface since the middle of the 19th century. *Marine Geology*, 234(1-4), 143-157.

Sabatier, F., Samat, O., Ullmann, A., Suanez, S., 2009. Connecting large-scale coastal behaviour with coastal management of the Rhône delta. *Geomorphology*, 107(1-2), 79-89.

Salvador, P.G., Berger, J.F., 2014. The evolution of the Rhône River in the Basses Terres basin during the Holocene (Alpine foothills, France). *Geomorphology*, 204, 71-85.

Schmedemann, N., Schafmeister, M.T., Hoffmann, G., 2008. Numeric de-compaction of Holocene sediments. *Polish Geological Institute Special Papers*, 23, 87-94.

Shackleton, N.J., Opdyke, N.D., 1973. Oxygen isotope and palaeomagnetic stratigraphy of Equatorial

Pacific core V28-238: Oxygen isotope temperatures and ice volumes on a 105 year and 106 year scale. *Quaternary research*, 3(1), 39-55.

Sharma, P.V., 1997. Environmental and engineering geophysics. Cambridge university press.

Smith, D.E., Harrison, S., Firth, C.R., Jordan, J.T., 2011. The early Holocene sea level rise. *Quaternary Science Reviews*, 30(15-16), 1846-1860.

Sornoza, L., Barnolas, A., Arasa, A., Maestro, A., Rees, J.G., Hernandez-Molina, F.J., 1998. Architectural stacking patterns of the Ebro delta controlled by Holocene high-frequency eustatic fluctuations, delta-lobe switching and subsidence processes. *Sedimentary Geology* 117(1-2), 11-32.

Stanley, D.J., 1997. Mediterranean Deltas: Subsidence as a Major Control of Relative Sea-Level Rise. *Bulletin Institut Océanographique*, 18, 35

Stanley, D.J., Warne, A.G., 1994. Worldwide initiation of Holocene marine deltas by deceleration of sea-level rise. *Science*, 265(5169), 228-231.

Stanley D.J., Warne A.G., 1998: Nile Delta in its destruction phase. *Journal of Coastal Research*, 795-825.

Stanford, J.D., Hemingway, P., Rohling, E.J., Challenor, P.G., Medina-Elizalde, M., Lester, A.J., 2011. Sea-level probability for the last deglaciation: A statistical analysis of far-field records. *Global and Planetary Change*, 79(3-4), 193-203.

Stefani, M., Vincenzi, S., 2005. The interplay of eustasy, climate and human activity in the late Quaternary depositional evolution and sedimentary architecture of the Po Delta system. *Marine Geology*, 222, 19-48.

Teatini, P., Gambolati, G., Castelletto, N., Ferronato, M., Janna, C., Cairo, E., Rocca, F., 2010. Monitoring and modelling 3-D ground movements induced by seasonal gas storage in deep reservoirs. *Proc. EISOLS*, 2010, 339.

Van Asselen, S., Stouthamer, E., Van Asch, T.W., 2009. Effects of peat compaction on delta evolution: a review on processes, responses, measuring and modeling. *Earth-Science Reviews*, 92(1-2), 35-51.

Van Wagoner, J.C., Posamentier, H.W., Mitchum, R.M.J., Vail, P.R., Sarg, J.F., Loutit, T.S. and Hardenbol, J., 1988. An overview of the fundamentals of sequence stratigraphy and key definitions. In: C.K. Wilgus, B.S. Hastings, C.G.St.C. Kendall, H.W. Posamentier, C.A. Ross and J.C. Van Wagoner (Editors), *Sea-Level Changes: An Integrated Approach*. Soc. Econ. Paleontol. Mineral., Spec. Publ., 42: 39-47.

Vauclin, S., Mourier, B., Tena, A., Piégay, H., Winiarski, T., 2020. Effects of river infrastructures on the floodplain sedimentary environment in the Rhône River. *Journal of Soils and Sediments*, 20, 2697-2708.

Vella, C., Fleury, T.J., Raccasi, G., Provansal, M., Sabatier, F., Brouniet, M., 2005. Evolution of the Rhône delta plain in the Holocene. *Marine geology*, 222, 235-261.

Vella, C., Fleury, T.J., Gensous, B., Labaune, C., Teston, M., 2008. Grandes séquences Holocènes et discontinuités sédimentaires dans le Delta du Rhône. Collection EDYTEM. *Cahiers de géographie*, 6(1), 155-166.

Vella, C., Tomatis, C., Sivan, O., 2014. Chapitre 3. Le contexte paléoenvironnemental. In: *Archaeonautica*, 18, 2014. Arles-Rhône 3. Un chaland gallo-romain du Ier siècle après Jésus-Christ. pp. 65-73; doi : <https://doi.org/10.5403/nauti.2014.1309>

Warne, A.G., Stanley, D.J., 1993. Archaeology to refine Holocene subsidence rates along the Nile delta margin, Egypt. *Geology*, 21(8), 715-718.

Wagner, S., Zorita, E., 2005. The influence of volcanic, solar and CO₂ forcing on the temperatures in the Dalton Minimum (1790–1830): A model study. *Climate dynamics*, 25, 205-218.

Wiles, G.C., D'Arrigo, R.D., Villalba, R., Calkin, P.E., Barclay, D.J., 2004. Century-scale solar variability and Alaskan temperature change over the past millennium. *Geophysical Research Letters*, 31(15).

Woodbridge, J., Roberts, N., Fyfe, R., 2018. Pan-Mediterranean Holocene vegetation and land-cover

dynamics from synthesized pollen data. *Journal of Biogeography*, 45(9), 2159-2174.

Yi, S., Saito, Y., Zhao, Q., and Wang, P., 2003. Vegetation and climate changes in the Changjiang (Yangtze River) Delta, China, during the past 13,000 years inferred from pollen records. *Quaternary Science Reviews*, 22(14), 1501-1519.

Zhao, J.B., Ma, Y.D., Cao, J.J., Hao, Y.F., Shao, T.J., Liu, X.M., 2020. Holocene pedostratigraphic records from the southern Chinese Loess Plateau and their implications for the effects of climate on human civilization, *Catena*, Volume 187,104410. ISSN 0341-8162. doi.org/10.1016/j.catena.2019.104410.

Zielhofer, C., Köhler, A., Mischke, S., Benkaddour, A., Mikdad, A., and Fletcher, W.J., 2019. Western Mediterranean hydro-climatic consequences of Holocene icerafted debris (Bond) events. *Climate of the Past*, 15, 463–475, <https://doi.org/10.5194/cp-15-463-2019>, 2019.

Zong, Y., Huang, K., Yu, F., Zheng, Z., Switzer, A., Huang, G., Tang, M., 2012. The role of sea-level rise, monsoonal discharge and the palaeo-landscape in the early Holocene evolution of the Pearl River delta, southern China. *Quaternary Science Reviews*, 54, 77-88.

Figure captions

Figure 1: Location of the study area. A) Rhône basin and its sub-basins, B) Location map based on a Google Earth image dated from 2016, showing the location of the different lobes described in the text, the location of the cores used to define the stratigraphic architecture of the Rhône delta, and location of the stratigraphic correlation transects.

Figure 2: Facies associations definition with dominant facies description, sequential organization, depositional processes, and figurative elements observed on the core analyzed in this study. The illustrations of the Facies Associations are taken from the three reference cores presented in Fig. 3 (FG, GMSC-1 and MD99-2352 cores).

Figure 3: Sedimentary description of 3 reference cores of the Rhône delta (FG, GMSC-1 and MD99-2352 cores), with Facies Associations interpretations, ^{14}C dates, facies, and sequential interpretation and stratigraphic cycles. FA for facies associations.

Figure 4: North–south stratigraphic correlation transect in the western part of the Rhône delta illustrating the S^t Ferréol and Peccaïs lobes architectures, including SC1, R1, FP3, KS04 and MD99 cores, respectively from proximal to distal. See Fig. 1 for location, and Table 1 for detailed information on the cores.

Figure 5: North–south stratigraphic correlation transect in the eastern part of the Rhône delta illustrating the Ulmet lobe architecture, including SC1, FG and KS40 cores from proximal to distal respectively. See Fig. 1 for location, and Table 1 for detailed information on the cores.

Figure 6: West–east stratigraphic correlation transect across the Rhône delta illustrating the architectures and geometrical relationships between the Peccaïs, S^t Ferréol, Ulmet, Bras de Fer and Roustan lobes, including FP3, R2, SF, FG, SG, 114, KS 27 and KS 51 cores. See Fig. 1 for location, and

Table 1 for detailed information on the cores.

Figure 7: Comparison of the stratigraphic correlation transects highlighting the different depositional units defined across the Rhône delta. Vertical scales have been harmonized.

Figure 8: Reconstructed topographic surface at 12500 Cal yr BP used as the basal surface for the sediment volume deposited calculation, including the ERDC.

Figure 9: Description of the steps used in estimating sedimentary volumes and flows of the Rhône delta system during the Holocene. A) Effects of decompaction in the delta plain and in the prodelta. The decompaction law used is that of Schmedemann et al., 2008, based on data from Gustavs, 1992; B) Quantification of the clays exported to the south and west, based on the reports of Got and Aloïsi, 1989, and Palanques et al., 2006; C) The steps of the volume to mass conversion that take into account only the solid fraction of the volume; D) Sediment flow during the distinct Holocene intervals defined in this study.

Figure 10: A: Evolution of the Rhône delta since the initiation of the Early Rhône Deltaic Complex at 12500 Cal yr BP, with flux and export for each period. B: Evolution of sediment flux into the deltaic system during the Holocene. Periods of rapid climate change (RCC) (Mayewski et al., 2004). Absolute sea level change (Jouet, 2007). Variation in flood frequency between the northern and southern Alps (Wirth et al., 2013).

Figure 11: Comparison of western Mediterranean deltas (Rhône, Pô and Ebro deltas) with eastern Mediterranean Nile delta, showing their sedimentary evolution, the eastern and western Mediterranean climatic context, and the sediment fluxes relative evolution during the Holocene. The Holocene climate evolution of the Western Mediterranean is reconstructed by the integration of published data from Jalut et al., 2000; Benito et al., 2015 and Katrantsiosi et al., 2019. The Holocene climate evolution in the Eastern Mediterranean is a compilation of published data from Zhao et al., 2020. The absolute sea-level curve is from Jouet et al., 2007, and the curves of summer and winter insolation at 40°N is from Magny 2013, modified from Berger and Loutre 1991. The Holocene

sedimentary flux curve of the Nile delta is a compilation of data published by Stanley and Warne, 1998 and Marriner et al., 2012. The Holocene sedimentary flux curve of the Pô delta is a compilation of data published by Corregiani et al., 2005. The Holocene sedimentary flux curve of the Ebro delta is a compilation of data published by Friogola et al., 2007 and Perez Lamban et al., 2018. The Holocene sedimentary flux curve of the Rhône is the result of this study.

Supplementary data

Table summarizing the sample dataset used for the datings, with the depth of each dated sample taken on cores, the type of sample, the ages including uncertainty, the publications where the data are available.

Table 1: Studied cores with location, core length, and radiocarbon dates realized in previous studies and published in peer reviewed articles, and datings made in this study to complete the existing dataset.

Cores	Research campaign	Year	Longitude	Latitude	Location	Length (m)	Datings (previous)	Datings (this study)
GMSC 1	Arles Rhone 3	2010	N 43°40.677	E 4°37.115	Apex	12.1	0	9
GMSC 1A	Arles Rhone 3	2010	N 43°40.677	E 4°36.998	Apex	17.6	3 (Vella & Sivan, 2014)	2
GMSC 8	Arles Rhone 3	2010	N 43°40.629	E 4°37.001	Apex	9.7	0	5
FG	GDR marges, Eurodelta	2004	N 43°27.513	E 4°37.200	Uinet	41.9	1 (Vella et al., 2005)	16
SF	GDR marges, ANR Armilit, Eurodelta	2007	N 43°29.871	E 4°25.858	Saint-Ferréol	45.2	19 (Vella et al., 2008)	1
FP3	GDR marges, ANR Armilit, Eurodelta	2007	N 43°22.835	E 4°14.245	Peccais	31.1	7 (Vella et al., 2008) 5 (Rey, 2006)	3
R1	N/A	2012	N 43°22.738	E 4°21.997	Saint-Ferréol	40	4 (Amorosi et al., 2013)	8
R2	N/A	2012	N 43°28.082	E 4°22.739	Saint-Ferréol	50	5 (Amorosi et al., 2013)	17
RHS-KS 04	Rhosos	2008	N 43°26.583	E 4°09.048	Prodelta	3.8	0	6
RHS-KS 21	Rhosos	2008	N 43°20.545	E 4°19.993	Prodelta	7.3	0	4
RHS-KS 27	Rhosos	2008	N 43°16.206	E 4°51.042	Prodelta	7.55	1 (Fanget et al., 2012)	3
RHS-KS 40	Rhosos	2008	N 43°17.939	E 4°30.479	Prodelta	7.8	10 (Fanget et al., 2012)	4
RHS-KS 51	Rhosos	2008	N 43°16.788	E 4°55.932	Prodelta	5.25	2 (Fanget et al., 2012)	4
RHS-KS 55	Rhosos	2008	N 43°14.354	E 4°40.961	Prodelta	7.3	14 (Fanget et al., 2012)	2

RHS-KS 57	Rhosos	2008	N 43°17.106 E 4°50.965	Prodelta	7.7	9 (Fanget et al., 2012)	1
BMKS 21	Beachmed	2004	N 43°20.582 E 4°24.344	Prodelta	5.55	7 (Berné et al., 2007)	3
MD99-2352	Images 5	1999	N 43°19.160 E 4°09.650	Prodelta	15.4	14 (Berné et al., 2007)	7
						94 dates	95 dates

Journal Pre-proof

Declaration of interests

The authors declare that they have no known competing financial interests or personal relationships that could have appeared to influence the work reported in this paper.

The authors declare the following financial interests/personal relationships which may be considered as potential competing interests:

Journal Pre-proof

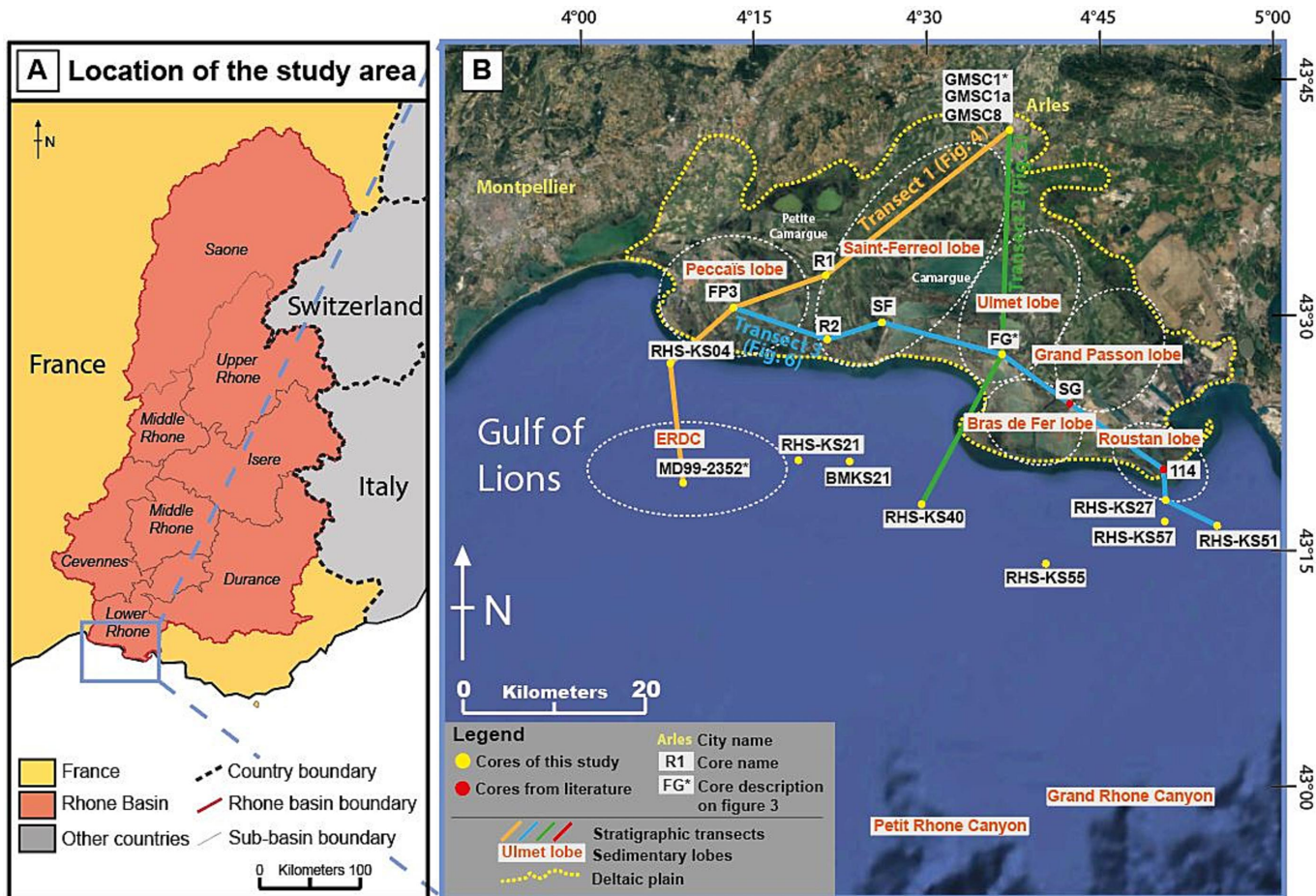


Figure 1





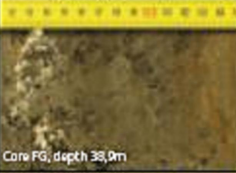
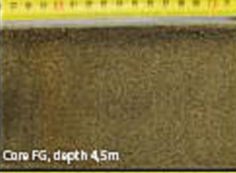


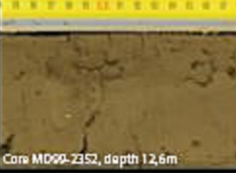
Facies Associations	Dominant facies	Sedimentary structures	Sequential organization	Depositional process	Figurative elements	illustration
C1 Alluvial plain	Very fine grained clayey-silty sandstones, poorly sorted. Rare floating granules and gravels, presence of roots	Rare current ripples, plane parallel laminations	Aggradation of silty-clay deposits, coarsening upwards decimetric sequences in the overflow deposits and crevasse lobes	Decantation, occasional unidirectional flood currents	Plant debris, roots	 Core GMSC-1, depth 1,3m
C2 Fluvial channel	Coarse to very coarse grained sandstone, very poorly sorted	Trough cross-stratification, current ripples	Erosive base, fining and thinning upwards	High energy tractive currents	Plant debris, roots	 Core GMSC-1, depth 19,3m
B1 Inner bay	Bioturbated clays or silty clays alternating with centimetric lenses of medium grained sands	Plane parallel laminations in the clays intervals, current ripples in the sandy lenses	Aggradation of clay deposits, alternating with sand lenses	Decantation of clays, low energy tractive currents for sand lenses, linked to flood events	Organic matter, wood fragments, shells of gastropods, bivalves	 Core FG, depth 40,5m
B2 Outer bay	Alternate of bioturbated clays/silt and fine grained sands with abundant mollusc shell fragments sometimes forming centimetric lags	Plane parallel laminations in the clays intervals, current ripples in the sandy lenses	Aggradation of clay deposits, alternating with sand lenses	Decantation of clays, low energy tractive currents for sand lenses, linked to flood events	Organic matter, rare wood fragments, abundant bivalve shells	 Core FG, depth 34,5m
MB Mouth bars/ Bay-head deltas	Fine to coarse grained sands, moderately sorted with abundant clay pebbles, bioturbated	Sigmoidal cross stratifications, sometimes	Organization in coarsening upwards sequences and thickening upwards	Dominant tractive currents	Clay pebbles, wood fragments, bioclast fragments	 Core FG, depth 38,0m
D1 Upper delta front	Very well sorted fine to medium grained sands	Plane parallel or low angle lamination	Organization in coarsening upwards and thickening upwards sequences	Wave current that reworks the sands brought by the river currents during floods	Rare bioclasts	 Core FG, depth 4,5m
D2 Lower delta front	Alternation of very fine bioturbated silty sands and with fine to medium grained sands of centimetric to decimetric in thickness	Frequent current ripples in bioturbated very fine grained sand intervals, hummocky cross-stratification	Organization in coarsening and thickening upwards sequences	Wave currents (storms) alternating with low energy tractive currents drifting from the river discharge	Rare wood fragments, bioclasts	 Core FG, depth 12,5m
M1 Prodelta	Bioturbated silty clays alternating with lenses of fine to very fine grained sand	Plane parallel laminations in silty clays, current ripples in sandy lenses	Organization in weakly coarsening upwards sequences	Decantation, low energy tractive currents related to river flooding	Rare bioclasts	 Core MD99-2352, depth 11 m
M2 Offshore	Bioturbated silty clays, with rare intra-centimeter sandy lenses	Parallel plane laminations	Sequences in aggradation	Decantation	Important bioturbation, rare bioclasts	 Core MD99-2352, depth 12,6m

Figure 2

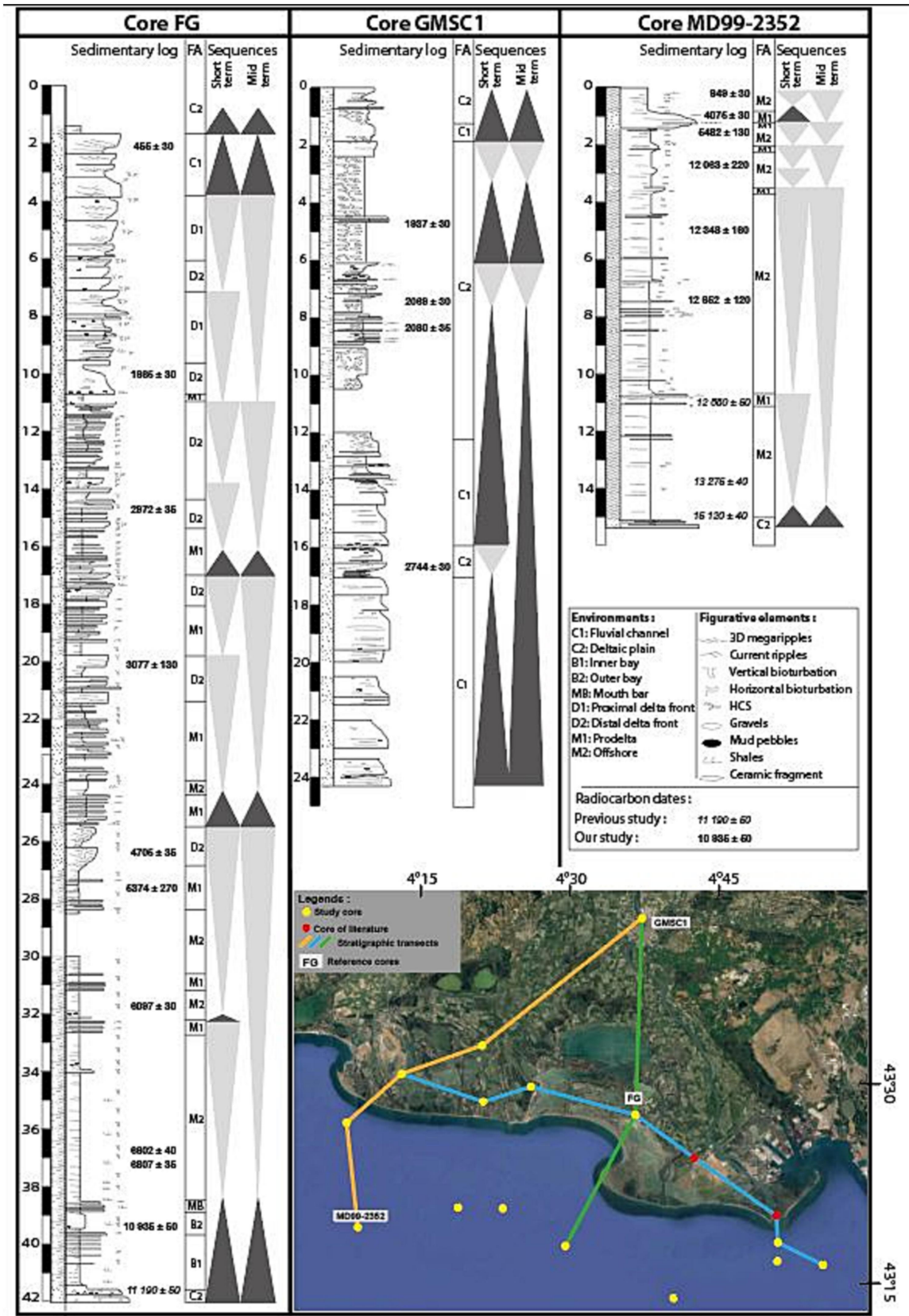


Figure 3

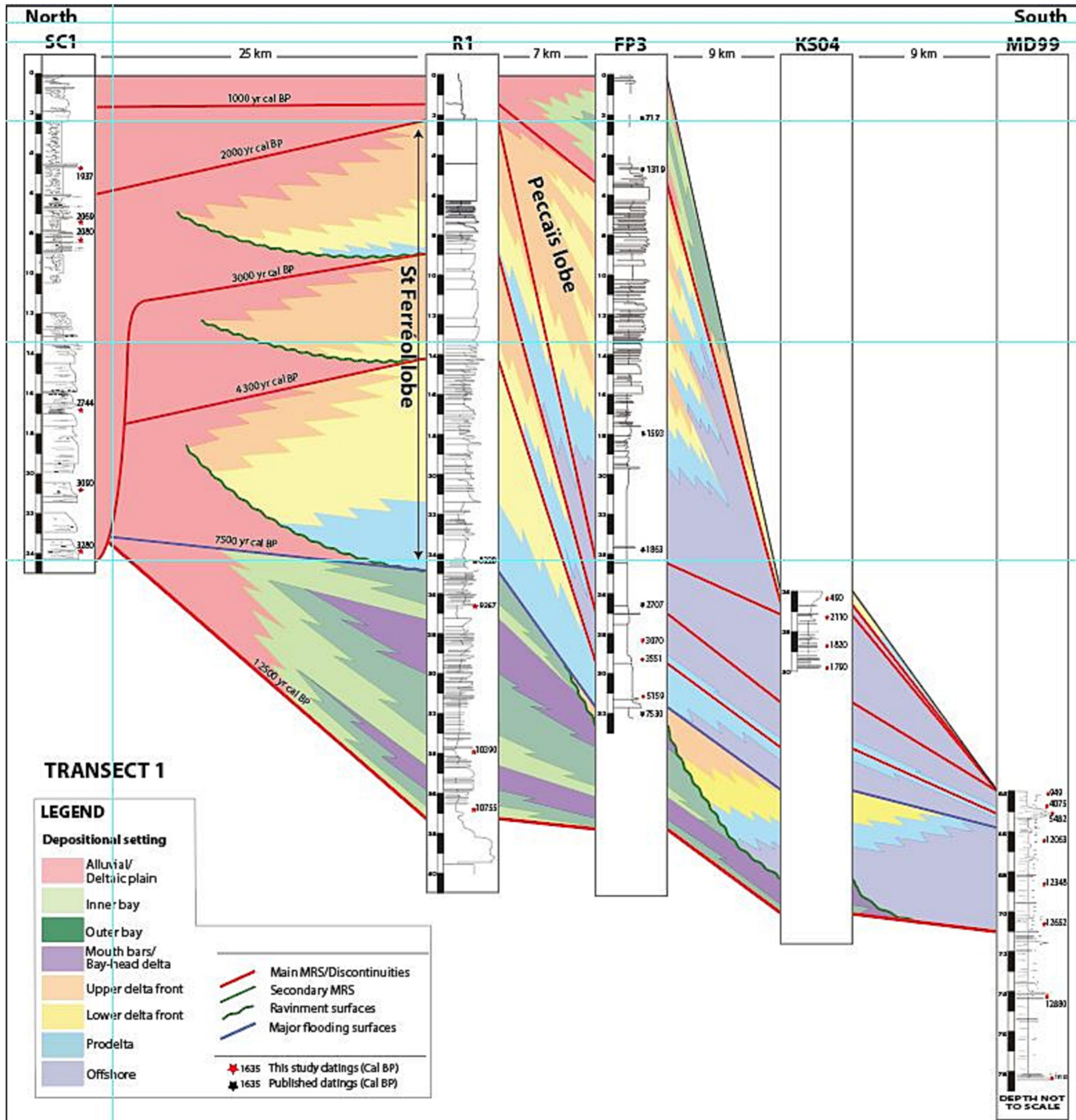


Figure 4

North
SC1

FG

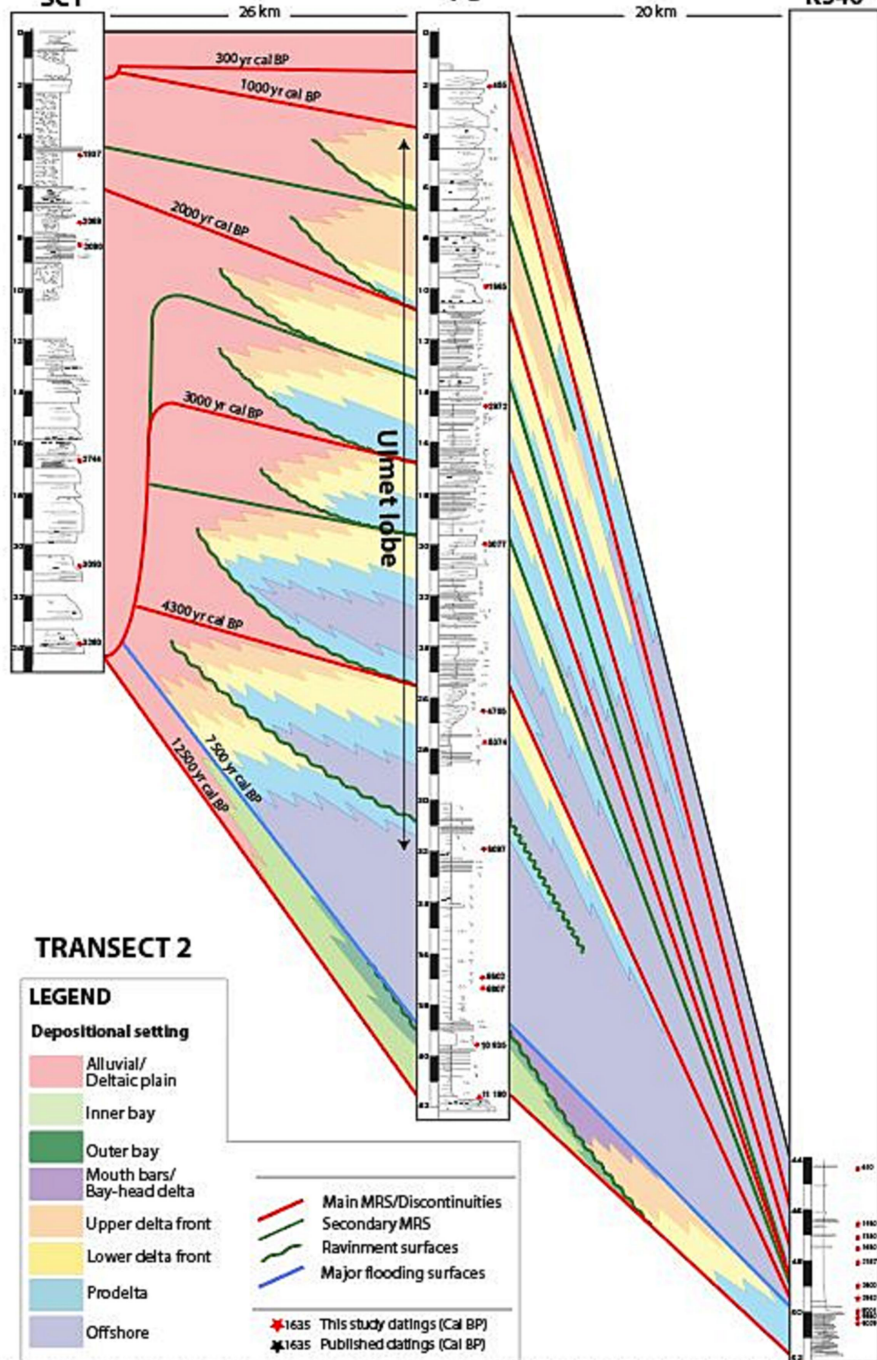
South
KS40

Figure 5

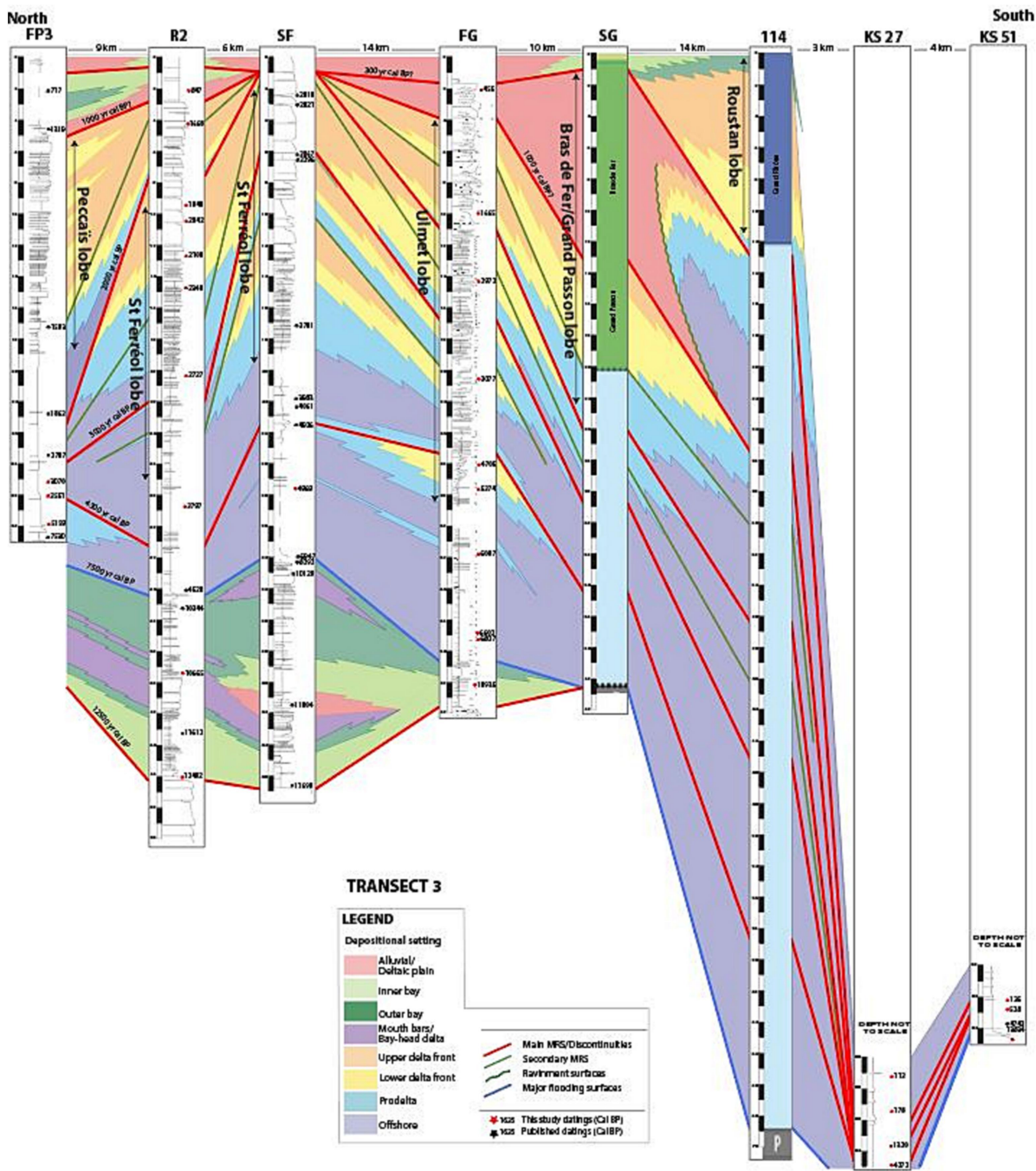


Figure 6

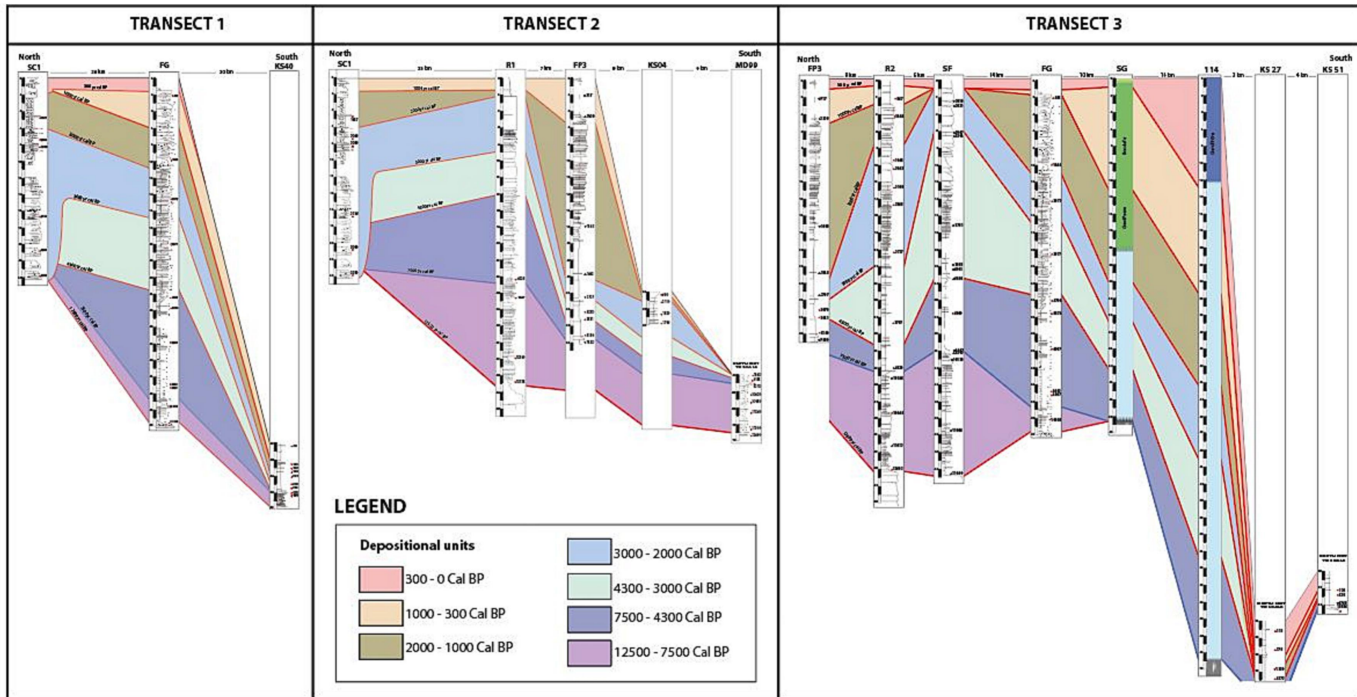


Figure 7

Initial Volume :
90 000 000 000 m³

Sediment decompaction :

A

Deltaic plain :
52 000 000 000 m³
Sand = 65%, Clay = 35%

Prodelta :
38 000 000 000 m³
Sand = 20%, Clay = 80%

60 000 000 000 m³

48 400 000 000 m³

$$\varphi(z) = \varphi_0 e^{-bz}$$

From Schmedemann et al., 2008

φ – recent porosity
 φ_0 – initial porosity
 b – compaction constant
 z – depth

Sediment	φ_0 [%]	b [1/km]	Source
Clay	82	25.00	Dietrich, 1989
Sand	49	0.27	Gustavs, 1992

C

Volume to mass conversion :

1m³ of clay = 495 kg
1m³ of sand = 1341 kg

Deltaic plain :

Prodelta :

60 000 000 000 m³
Sand = 65%, Clay = 35%
+ Clays export

48 400 000 000 m³
Sand = 20%, Clay = 80%
+ Clays export

65 800 000 000 tons

39 400 000 000 tons

Total mass :

105 200 000 000 tons +- 10%
95 000 000 000 to 115 000 000 000 tons

B

Sediment (clays) export :

30 % exported
(Got & Aloisi, 1989)

17 700 000 000 m³ +- 10%

25% export to the West
(Palanques et al., 2006)

14 700 000 000 m³ +- 10%

5% export to the South
(Palanques et al., 2006)

3 000 000 000 m³ +- 10%

Total volume :

126 100 000 000 m³ +- 10%

D

Fluxes by Holocene key interval :

<i>Period</i>	<i>Volume</i>	<i>Sand</i>	<i>Clay</i>	<i>Sand (Mt)</i>	<i>Clay (Mt)</i>	<i>Flux (Mt/yr)</i>
0 - XVIII :	4%	2%	2%	2104	2104	14.0
XVIII - 1000 :	17%	10%	7%	10520	7364	25.5
1000 - 2000 :	15%	8%	7%	8416	7364	15.8
2000 - 3000 :	20%	11%	9%	11572	9468	21.0
3000 - 4100 :	8%	3%	5%	3156	5260	7.7
4100 - 7000 :	15%	5%	10%	5260	10520	5.4
7000 - 12500 :	21%	9%	12%	9468	12624	4.0
0 - 12 500 :	100%	48%	52%	50496	54704	8.4

Figure 9

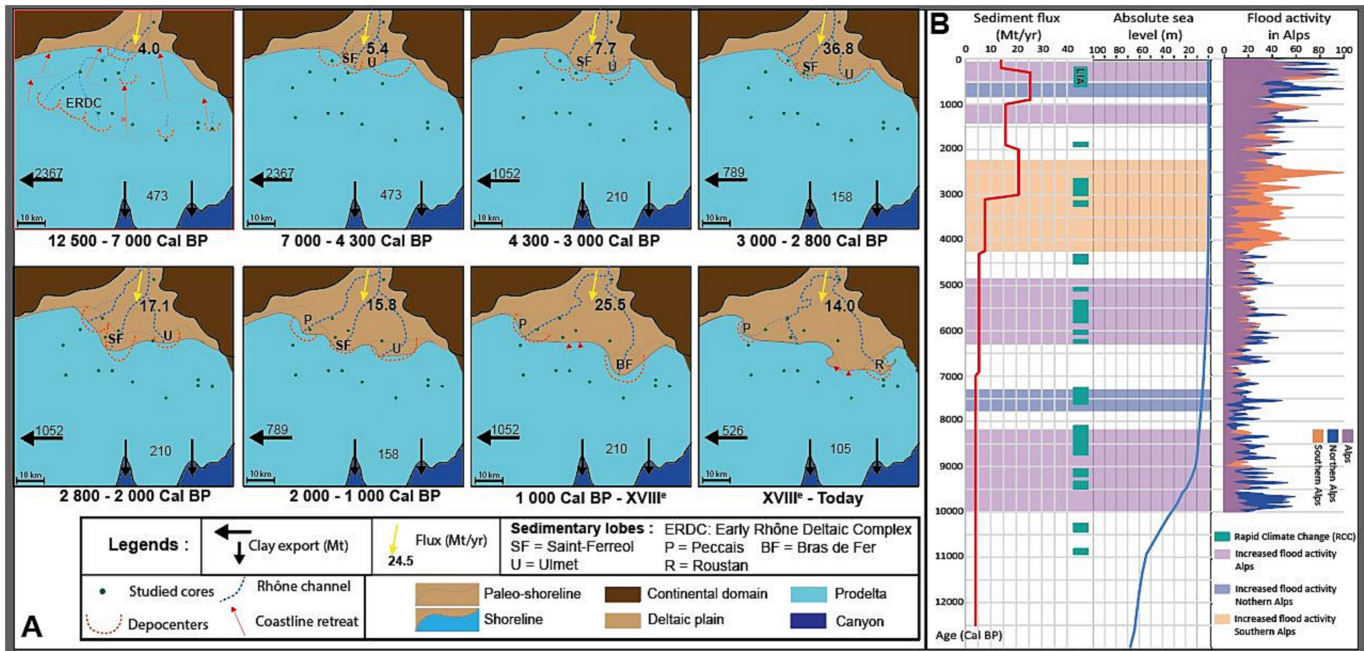


Figure 10

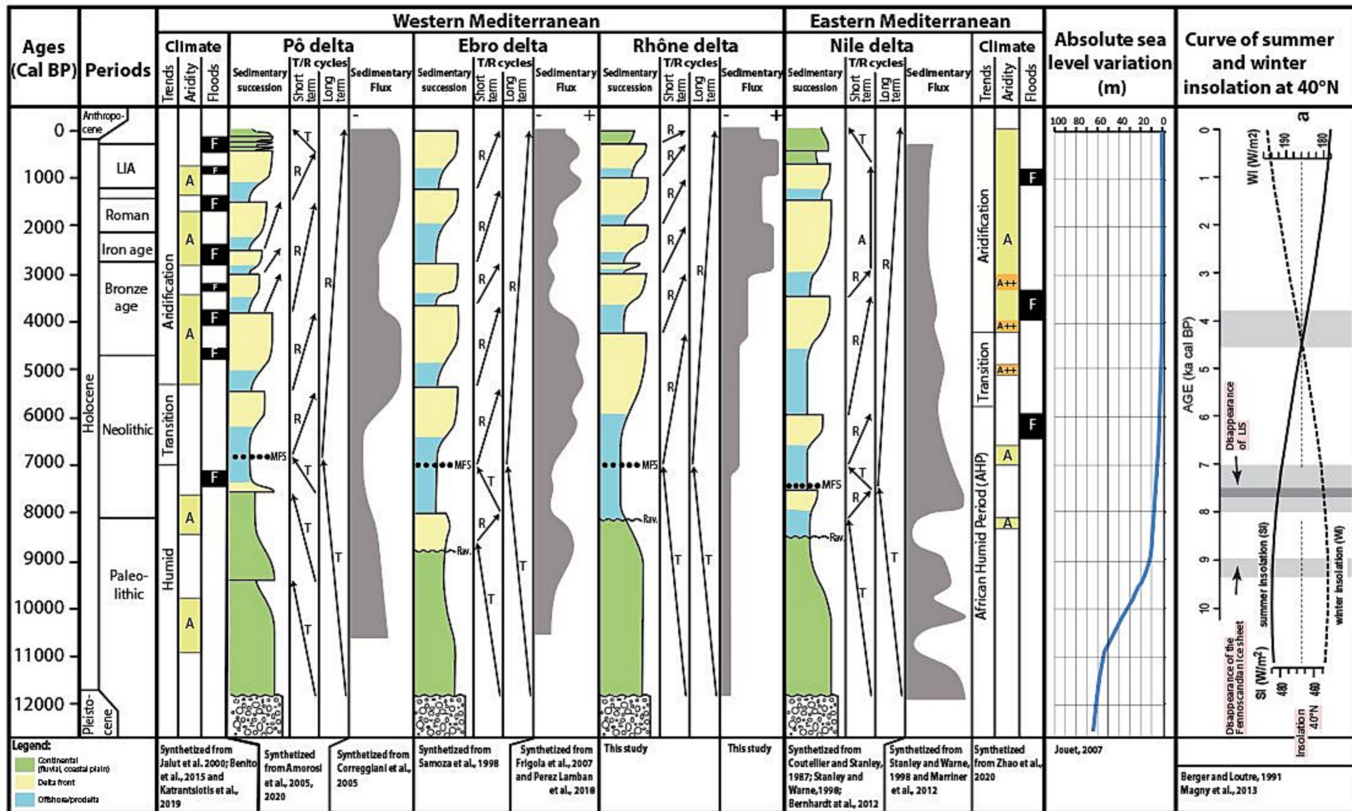


Figure 11